Edwards, B., Ktenidou, O.-J., Cotton, F., Abrahamson, N., Van Houtte, C., Fäh, D. (2015): Epistemic uncertainty and limitations of the κ0 model for near-surface attenuation at hard rock sites. - *Geophysical Journal International*, *202*, 3, p. 1627-1645.

DOI: http://doi.org/10.1093/gji/ggv222

Geophysical Journal International

Geophys. J. Int. (2015) **202,** 1627–1645
GJI Seismology

doi: 10.1093/gji/ggv222

Epistemic uncertainty and limitations of the κ_0 model for near-surface attenuation at hard rock sites

Benjamin Edwards,[1,2] Olga-Joan Ktenidou,[3] Fabrice Cotton,[3] Norman Abrahamson,[4] Chris Van Houtte[5] and Donat Fäh[1]

[1]*Swiss Seismological Service, ETH, Zürich, Switzerland. E-mail: ben.edwards@liverpool.ac.uk*
[2]*Department of Earth, Ocean and Ecological Sciences, University of Liverpool, Liverpool, United Kingdom*
[3]*ISTerre, Université de Grenoble* 1, *CNRS, F-*38041 *Grenoble, France*
[4]*Department of Civil and Environmental Engineering, University of California, Berkeley, CA, USA*
[5]*Department of Civil Engineering, University of Auckland, Auckland, New Zealand*

Accepted 2015 May 27. Received 2015 May 22; in original form 2014 November 24

SUMMARY

The determination of near-surface attenuation for hard rock sites is an important issue in a wide range of seismological applications, particularly seismic hazard analysis. In this article we choose six hard to very-hard rock sites (Vs_{30} 1030–3000 m s^{-1}) and apply a range of analysis methods to measure the observed attenuation at distance based on a simple exponential decay model with whole-path attenuation operator κ_r. The κ_r values are subsequently decoupled from path attenuation (Q) so as to obtain estimates of near-surface attenuation (κ_0). Five methods are employed to measure κ_r which can be split into two groups: broad-band methods and high-frequency methods. Each of the applied methods has advantages and disadvantages, which are explored and discussed through the comparison of results from common data sets.

In our first step we examine the variability of the individual measured κ_r values. Some variation between methods is expected due to simplifications of source, path, and site effects. However, we find that significant differences arise between attenuation measured on individual recordings, depending on the method employed or the modelling decisions made during a particular approach. Some of the differences can be explained through site amplification effects: although usually weak at rock sites, amplification may still lead to bias of the measured κ_r due to the chosen fitting frequency bandwidth, which often varies between methods. At some sites the observed high-frequency spectral shape was clearly different to the typical κ_r attenuation model, with curved or bi-linear rather than linear decay at high frequencies. In addition to amplification effects this could be related to frequency-dependent attenuation effects [e.g. $Q(f)$]: since the κ_r model is implicitly frequency independent, κ_r will in this case be dependent on the selected analysis bandwidth.

In our second step, using the whole-path κ_r data sets from the five approaches, we investigate the robustness of the near-surface attenuation parameter κ_0 and the influence of constraints, such as assuming a value for the regional crustal attenuation (Q). We do this by using a variety of fitting methods: least squares, absolute amplitude and regressions with and without fixing Q to an *a priori* value. We find that the value to which we fix Q strongly influences the near-surface attenuation term κ_0. Differences in Q derived from the data at the six sites under investigation could not be reconciled with the average values found previously over the wider Swiss region. This led to starkly different κ_0 values, depending on whether we allowed for a data-driven Q, or whether we forced Q to be consistent with existing simulation models or ground motion prediction equations valid for the wider region. Considering all the possible approaches we found that the contribution to epistemic uncertainty for κ_0 determination at the six hard-rock sites in Switzerland could be represented by a normal distribution with standard deviation $\sigma\kappa_0 = 0.0083 \pm 0.0014$ s.

Key words: Earthquake ground motions; Site effects; Wave propagation.

1 INTRODUCTION

Seismic attenuation describes the reduction in amplitude of seismic waves during their propagation due to processes such as internal friction, scattering and geometrical spreading. The determination of this phenomenon plays an important role in a range of seismological applications, such as probabilistic and deterministic seismic hazard analysis, magnitude determination, source characterization and site response analysis. Ultimately, engineers and seismologists wish to know the proportion of an earthquake's source energy that will reach a target location. Beyond other wave propagation effects (e.g. guided waves, reflected waves and surface waves) it is attenuation that controls this behaviour.

It is common to observe that recordings of earthquakes at the earth's surface lack high-frequency energy, even when recorded at relatively close distances. On the other hand, simple models of energy radiated from earthquakes (e.g. Brune 1970) show that there should be a constant level of Fourier spectral acceleration radiated at all frequencies above the earthquake's source corner frequency. The disparity between these simple source models and observations was explained by Hanks (1982) as the f_{max} effect, with f_{max} describing the high-frequency band-limitation of the radiated ground-motion field of earthquakes. Anderson & Hough (1984) later introduced the concept of κ: a low-pass filter in the form of an exponential decay model. Both authors attributed these concepts to site (and in the case of Anderson and Hough also weakly to propagation) rather than source effects. The similarity to seismic attenuation described by Q (Knopoff 1964), which is also modelled using exponential decay, is obvious, although other authors have also explored the notion of a source-based effect filtering out high frequencies of strong ground motion (Papageorgiou & Aki 1983).

In most studies, the observed low-pass filtering between the source and site is attributed to damping in the upper crustal rock and the soil layers. The mechanism for this is not clear, but may simply be related to low-Q materials in the near-surface. The most convincing evidence of the site's influence is from dual surface-borehole instrumentation where this effect can be seen through spectral ratios and is thus only attributable to the upper layers (e.g. Abercrombie 1997). The path-corrected component of κ_r, the so-called κ_0, is therefore typically thought of as an 'observed' site characteristic: quantifying attenuation related to near-vertical wave propagation in the upper rock or soil layers. It is determined from the individual whole path attenuation (κ_r) values at a particular site, after observing their dependence with distance from the source. Often this dependence can be considered to be linear, and thus a simple regression of measured κ_r versus distance will yield κ_0 as the zero-distance intercept. This linear trend between attenuation and distance indicates limited depth dependence of κ_r (e.g. Edwards *et al.* 2011) since varying Q with depth manifests as curvature in the κ_r versus distance plots (Hough & Anderson 1988; Hough *et al.* 1988). It has been noted that if a simple straight line form does not fit the data, any other smooth functional form could be used (Anderson 1991). The intersection of the function at zero distance is then κ_0. However, increased complexity in the distance dependence leads to increased uncertainty in extrapolating to zero-distance (where data is not typically available) and thus determining κ_0.

1.1 Impact of κ_0 in seismic hazard

In seismic hazard analysis projects, ground motion prediction is typically performed at a rock or hard-rock reference [e.g. in the case of Switzerland, at 1105 m s^{-1} (Poggi *et al.* 2011)]. Site-specific non-linear amplification is then applied to the input rock prediction in a subsequent stage. This allows more detailed and complex site-specific hazard to be computed than by simply using a proxy (e.g. Vs_{30}) within the ground motion prediction equation (GMPE) itself. However, the prediction of ground motion at a rock reference adds significant uncertainty: for instance, in the case of hard-rock using the reference site's Vs_{30} directly in a GMPE is not favoured, since GMPEs are typically poorly constrained at high Vs_{30} values due to lack of data on hard rock. In fact, since GMPEs are typically developed using data dominated by recordings on stiff-soil sites (e.g. Vs_{30} 300–700 m s^{-1}), they may not adequately represent the rock reference (typically $Vs_{30} \gtrsim 800$ m s^{-1}) desired for seismic hazard. Host-to-target adjustment of GMPEs must therefore be considered for such sites. This aims to translate a model (in this case using Vs_{30} that produces sufficiently robust and reliable predictions), including its uncertainty, to provide predictions at a specific reference site (Campbell 2003), usually on rock or hard rock.

While amplification effects must be considered for host-to-target adjustment, at high frequencies the dominant effect for hard-rock sites (after considering the related uncertainty) is due more to site attenuation than to site amplification (Laurendeau *et al.* 2013). The selection of host and target κ_0 will therefore play a dominant role in the adjustment of GMPEs from moderate Vs_{30} to hard-rock predictions. Numerous authors have shown that the κ_0 term varies significantly from site to site and region to region (e.g. Edwards *et al.* 2008; Campbell 2009; Edwards & Rietbrock 2009), with several authors (e.g. Silva *et al.* 1998; Chandler *et al.* 2006; Edwards *et al.* 2011; Van Houtte *et al.* 2011; Poggi *et al.* 2013) also showing a weak correlation between Vs_{30} and κ_0. Correlations of κ_0 to site-proxies such as Vs_{30} are often used to infer κ_0 for hard-rock sites. However since empirical evidence of hard-rock κ_0 is severely lacking, these are poorly constrained, making the selection of host and target κ_0 difficult. Furthermore, the measurement method and the region studied may increase uncertainty in such correlations, highlighting the need for further investigation (Ktenidou *et al.* 2014).

An example of this is the Pegasos Refinement Project, a Senior Seismic Hazard Analysis Committee (SSHAC 1997) level 4 hazard analysis of Swiss nuclear power plants. GMPEs determined using data from around the world were used; however they were considered valid only at a range of 'reference Vs_{30} values': expert elicitation determined that the GMPEs did not properly extrapolate to high Vs_{30} values, since no, or insufficient, κ_0 variation with Vs_{30} was present when applying the Inverse Random Vibration Theory approach (Al Atik *et al.* 2014). In order to predict ground motion at the adopted Swiss rock reference site and maintain unbiased predictions, the GMPEs were therefore adjusted from host sites with Vs_{30} at which the models and associated metadata were considered sufficiently robust based on, for example, data coverage. This equated to $Vs_{30} \approx 600$ to 700 m s^{-1} and corresponding $\kappa_0 \approx 0.03$–0.04 s across the range of GMPEs. The target reference to which the GMPEs were converted had $Vs_{30} = 1105$ m s^{-1} with $\kappa_0 \approx 0.016$–0.022 s (Renault 2014). Correcting for κ_0 involves exponential attenuation functions and is sensitive to both host and target: the wide range of possible values in both host and target therefore introduced significant epistemic uncertainty in the final seismic hazard. Determining precise and accurate κ_0 values is thus critical to reduce uncertainty in rock-reference seismic hazard.

The aim of this study is to estimate κ_0 for rock sites and investigate the contribution of method choice and modelling assumptions to epistemic uncertainty through the use of different methods and approaches, including different data selection and modelling options

within each method. The analysis will enable us to present a range of κ_0 values for hard rock sites, which can be used to supplement existing empirical correlations (e.g. Vs_{30} to κ_0) at high Vs values, where their scatter is particularly large. The results of this study will be important for characterizing hard rock sites, particularly in stable continental regions, and could be useful for calculating input ground motions in site specific (e.g. critical facility) hazard.

Several established methods are available to determine κ_0 (Ktenidou *et al.* 2014). In order to investigate the variability of measured κ_r and κ_0 and therefore the robustness of applications using them, we apply two groups of approaches that we deem appropriate for the data set at hand. The first involves the analysis of the high-frequency part only (i.e. above the source corner frequency), while the second involves broad-band modelling of the Fourier spectrum of earthquake recordings. We will refer to these approaches the acceleration spectrum (AS) and the broad-band (BB) approach in short. Six very hard rock sites of the Swiss Digital Seismic Network (SDSNet), which exhibit only limited or no amplification, form the subject of this detailed analysis.

2 RECORDING SITES AND DATA

We use data from the SDSNet (Deichmann *et al.* 2010) of the Swiss Seismological Service (SED). Six very hard rock sites (Vs_{30} ranging from 1000–3000 m s^{-1}) were selected from across Switzerland (Fig. 1). Each site shows either negligible or limited amplification, particularly in the high-frequency range, as shown in Fig. 2. The amplification in these plots was computed from earthquake recordings by Edwards *et al.* (2013) using an approach based on the spectral analysis of regional seismicity. The approach effectively looks for systematic trends in the residual misfit of earthquake Fourier spectra to a reference rock model—interpreting repeated effects at a given site as site amplification. Non-linear effects are not considered, but due to the small size of earthquakes and hard rock sites considered in this study site effects are assumed to be entirely linear. The amplification is relative to the regional reference velocity model of Poggi *et al.* (2011). In addition to direct estimates of amplification, the absence of spectral peaks in horizontal to vertical (H/V) spectral ratios also confirmed that limited amplification would be present at these sites (Fäh *et al.* 2001).

We used earthquakes from Switzerland and its surrounding regions, spanning the period 1999–2009, with M_L computed by the SED greater than 2 (the data set is described in more detail by Edwards *et al.* 2011). The total number of records at the six sites with acceptable SNR on at least one component was 3433, with records per site ranging from 193 to 405. 16 per cent of the records were from stations within 50 km of the source, 31 per cent within 50–100 km and 53 per cent at distances greater than 100km. All sensors are STS-2 (Deichmann *et al.* 2011) with a sampling rate of 120 Hz (Nyquist frequency 60 Hz). The response of the STS-2 is mostly flat up to 30 Hz. All waveforms were therefore corrected for the instrument response and used up to 30 Hz (which is also below the effect of strong anthropogenic noise). Subsequent processing of the waveforms was then undertaken separately by the two first authors in order to reflect the differences that may arise from decisions such as window lengths, filtering, etc. This can be considered as a way to help understand epistemic uncertainty, as the estimation of κ_r can be method-dependent as well as user-dependent (Ktenidou *et al.* 2013). For instance, the selected frequency ranges to be fit are often subjective.

The processing for the broadband (BB) and automatic high-frequency (hereinafter AS auto) approaches follows that described in Edwards *et al.* (2011) and is repeated briefly here. Waveforms are first windowed to provide signal and noise estimates. If *S*-wave arrivals are not available, a *P*:*S* velocity ratio of 1.73 is used to estimate the arrival time from manual *P*-wave picks. The signal window duration and position encapsulate 5 to 95 per cent of the cumulative squared velocity around the *S* waves ($T_{v,5-95\%}$). Both signal and noise windows are demeaned and tapered using multitaper algorithms (Lees & Park 1995) with 5 3π-prolate tapers, before applying a fast Fourier transform (FFT) and multiplying by the sampling period to obtain the two-sided Fourier spectrum of each record. A signal-to-noise ratio (SNR) analysis selectively defines the valid frequency range for each individual recording. In order to extract only the most reliable data, the noise estimate is conservatively increased, if necessary, to the extent that the signal and noise intersect at both the lowest and highest available frequencies of each spectrum. The useful frequency range is then defined for each recording as where the signal-to-noise ratio is greater than 3 over a continuous bandwidth of at least a decade of frequency (e.g. 1–10 Hz, 2–20 Hz, etc.). After performing the SNR analysis, spectra with lowest usable frequencies above 5 Hz, or highest useable frequencies lower than 10 Hz were discarded in order to maintain bandwidth across the range of frequencies of interest.

For the manual high-frequency (AS) method (hereinafter AS manual), the velocity waveforms were first corrected for mean and trend, then tapered at the edges using a Hanning window of 5 per cent width, and converted to acceleration through differentiation. *P* and *S* wave arrivals were picked visually, observing velocity and acceleration traces for all three components using different filters. Following that, noise and *S*-wave windows were chosen visually, also taking into account for the latter the magnitude and distance of the events. For records with small magnitudes and distances, we kept a minimum nominal duration of 5 s in the interest of adequate spectral resolution. Records of obvious poor quality (late *S* triggers, high noise level, double events) were discarded. Noise and *S*-wave windows were re-tapered with a Hanning window of 2.5 per cent width and then the FFT was applied. Only amplitude spectra (FAS) of acceleration were retained. A SNR check was performed after the initial visual selection of the frequency band (from f_1 to f_2) over which κ_r was computed. f_1 and f_2 were subsequently adjusted to ensure SNR > 3.

3 METHODS FOR DETERMINING κ_0

3.1 Broad-band Fitting (κBB approach)

The first method used to determine the attenuation along the wave path is a broad-band inversion approach (e.g. Masuda & Suzuki 1982; De Natale *et al.* 1987; Scherbaum 1990). We follow the inversion approach detailed in Edwards *et al.* (2008), aiming to fit the visible spectral bandwidth with a simple earthquake far-field point-source model (Brune 1970), defined by its source-corner frequency (f_c) and seismic moment (M_0), and the κ_r parameter. We note here that the t^* term (e.g. Rietbrock 2001), explicitly related to attenuation due to Q along the ray path and κ_r (the measured deviation from a ω^2 high-frequency Fourier displacement amplitude decay) are synonymous in our application, since we attribute all filtering effects to frequency independent Q [to be consistent with the AS approach (Anderson & Hough 1984)] and none to the source (Hough *et al.* 1988; Anderson 1991).

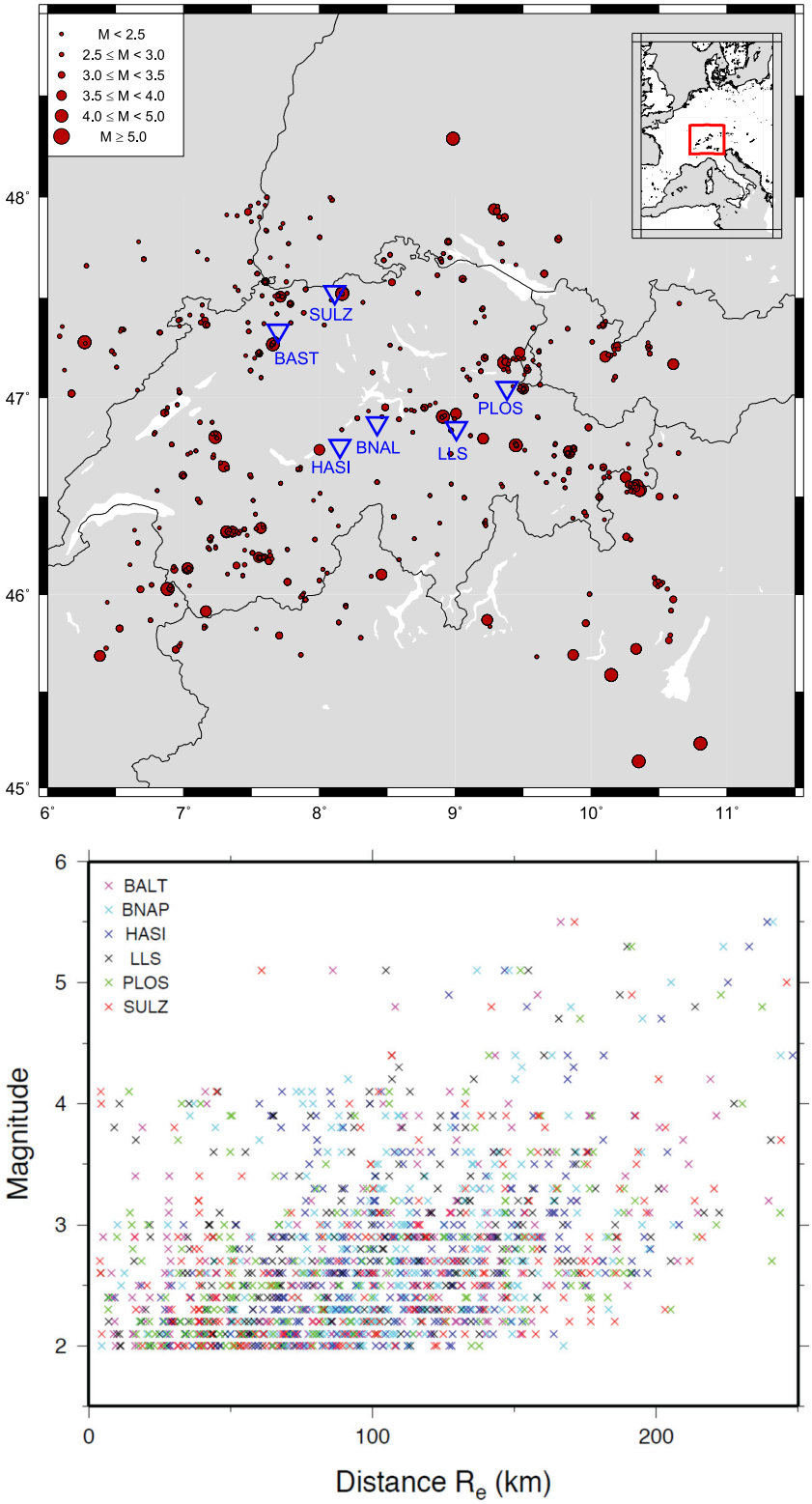

Figure 1. Station and epicentre distribution (top panel), and epicentral distance (R_{epi}) – local magnitude (M_L) distribution of records (bottom panel). Station labels: BALST (BALT); BNALP (BNAP); HASLI (HASI); PLOS (PLONS); LLS (LLS); SULZ (SULZ).

Even for hard and very hard rock sites, crustal amplification, associated to the reduction in shear-wave velocity between earthquake source depths (typically several kilometres) and the surface could pose a problem for the broad-band approach (Fig. 3). The shape of such amplification is typically a ramp function due to the relatively smooth velocity gradient with depth, with the step in amplification occurring over relatively low frequencies (e.g. ∼0.1 to 1–5 Hz). The hard-rock reference amplification function of Poggi *et al.* (2011) (Fig. 3), derived for Switzerland, was therefore removed from the spectra before inverting using the BB approach. Note that for the

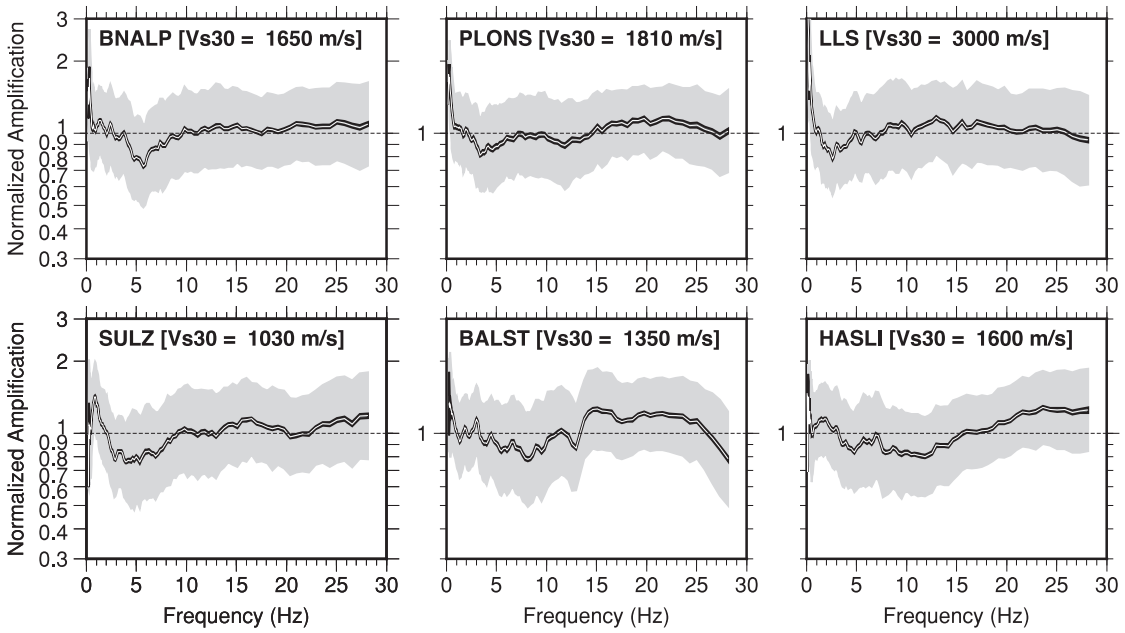

Figure 2. Observed amplification with respect to the Swiss rock reference model of Poggi *et al.* (2011) at the six sites under study. The amplification functions are normalized by a constant factor such that the average amplification is unity to highlight amplification shape. The line indicates the mean (with thickness ± one standard error), and the shaded grey area shows ± one standard deviation.

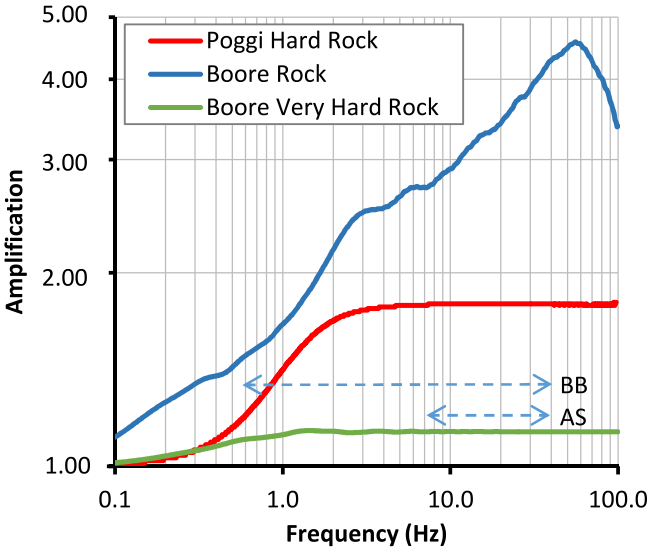

Figure 3. Examples of amplification expected for hard and very-hard rock conditions ($Vs_{30} = 1105\,\mathrm{m\,s^{-1}}$, Poggi *et al.* (2011) and $Vs_{30} = 2200\,\mathrm{m\,s^{-1}}$, Boore & Joyner (1997), respectively) and that for a generic rock condition ($Vs_{30} = 620\,\mathrm{m\,s^{-1}}$; Boore & Joyner 1997). Typical fitting frequency bandwidths for broad-band (BB) and high-frequency (AS) methods are indicated.

AS approaches the Swiss hard rock amplification does not have a significant effect, as it is broadly flat (not changing in amplitude with frequency) in the frequency range of interest. We therefore do not remove it for the AS methods. However, for amplification that does not plateau after a relatively low frequency (e.g. for lower velocity rock sites, Fig. 3), or for large earthquakes (with source corner-frequencies below the end of the ramp), it would be important to either account for amplification or only fit above frequencies which are affected.

In the BB inversion approach of Edwards *et al.* (2008), f_c is event-specific: f_c is simultaneously fit for all recordings of one event. The justification for this is to stabilise the inversion, limiting any biasing effect of unmodelled or non-parametric effects, such as site amplification. However, here we also test a record-specific apparent f_c, which leads to a better fit of the modelled spectra to the data (more degrees of freedom), at the expense of potentially unjustified variability in the source terms and lack of control of the influence of the site term. A specific risk is related to the strong trade-off between the source (f_c) and the site (κ_0; Boore *et al.* 1992), which means that the apparent f_c may be masked by attenuation (κ_r).

3.2 High-frequency linear fitting (κAS approach)

The second method we use for estimating κ_r is the high-frequency (AS) approach introduced by Anderson & Hough (1984), a review of which was given by Ktenidou *et al.* (2013). The method is to fit a straight line with gradient equal to $-\pi\kappa_r$ to the Fourier acceleration spectrum, in log-linear space. The frequency range over which κ_r is measured is from f_1 (which should lie above the source corner frequency) and f_2, which should lie below the frequency at which the noise floor begins. Given the large scatter found by Ktenidou *et al.* (2013) between different applications of this method, we use two approaches to do this: a completely manual, seismologist-reviewed approach, and a completely automatic approach. For the reviewed approach we checked each spectrum visually to find the minimum (f_1) and maximum (f_2) fitting frequencies. For the automatic approach we use only events with $M_L > 3.5$ and set the minimum value of f_1 at 10 Hz noting that $f_c = 10$ Hz is equivalent to a stress drop of approximately 10 MPa at $M_w = 3.5$ (with higher stress drops leading to higher f_c). This is conservatively high compared to values previously determined for Switzerland (Bay *et al.* 2005; Edwards & Fäh 2013b). After visually picking f_1 and f_2, we then only keep the frequency band between them for which SNR exceeds 3. SNR is computed from the FAS of the *S* wave and noise windows after smoothing them with a Konno & Ohmachi (1998) filter. In both cases κ_r was then determined using a least-squared (L2) regression on the FAS between f_1 and f_2. For each record there

are two measurements, one for each horizontal component. Based on the assumption of a single (isotropic) site- and path-specific κ_r, we average those to derive a single value per record for the AS approach.

3.3 Deriving a model for Q and κ_0

After the individual κ_r values are measured, we first verified that they have a broadly linear dependence with distance, such that the simple linear relation between distance and κ_r (Anderson & Hough 1984) could be applied. We made this check visually and also using a non-parametric inversion scheme, neither of which revealed any significant deviation from the linear model. We use certain quality criteria in order to choose which κ_r values to use in the regressions for Q and κ_0, which will yield the final κ models (i.e. for a linear regression, κ_0 and frequency-independent Q). These criteria include the following considerations:

(1) Defining a minimum spectral range in which to fit κ_r (e.g. $f_2 - f_1 = \Delta f > 8$ Hz).
(2) Accepting or rejecting negative κ_r values.
(3) Setting a threshold for the difference in the two horizontal components (e.g. $\Delta\kappa_r < 50$ per cent).
(4) Removing small magnitude events altogether (e.g. $M < 2.5$ or 3) to avoid trade-off of κ_r with the source f_c.

After selecting the κ_r data, we investigate two ways to regress with distance in terms of Q constraints: fixing Q to the value of the Swiss stochastic ground motion model (Edwards & Fäh 2013b), that is, using external information; or using the ensemble of the six stations studied here to estimate Q, that is, allowing the data to determine it. The fixed value of the stochastic model is $Q = 1200$, while the data-driven value, as shown in the following sections, is on average 1950, with a range from around 1600 to 2400 depending on the quality criteria applied. Following these two different approaches will allow us to evaluate the contribution of these choices to epistemic uncertainty in Q and its effect on the uncertainty of κ_0 given the trade-off between the two.

4 RESULTS OF κ_r ANALYSES

The initial analysis of FAS using the different methods provides a measure of κ_r: the argument to the exponential $\exp(-\pi f \kappa_r)$ used to fit the spectrum recorded at distance. Before proceeding with the determination of site-specific κ_0, we first compare the direct spectrum measurements κ_r. In an initial step we verified that the differences in κ_r between the different methods, reflecting a contribution to the epistemic uncertainty in this parameter, could be described by a normal-distribution with lin-space κ_r (Fig. 4). As a consequence the uncertainties in this paper are presented in terms of absolute differences in κ_r and κ_0, rather than ratios or percentages. While this implies that negative κ_r are possible, especially for hard-rock sites, we must consider that κ_r is an empirical parameter, and is in reality influenced not only by near-surface attenuation, but also the deviation from the Brune ω^2 model that is implicitly assumed when measuring κ_r, along with other unmodelled effects.

4.1 Comparison of κ_r AS approaches

The first comparison is where we expect the best correspondence—using the high-frequency fitting (AS) method with (1) manually reviewed spectra (AS manual) and (2) automatically processed spectra (AS auto). Since we compare common measures, this limits the comparison to events with $M > 3.5$ (the minimum magnitude used for the automatic method), which should represent a best-case scenario in terms of minimizing the trade off with source-corner frequency. In Fig. 5 we see that the correspondence at station LLS (the best case) is very good, with a difference (AS manual–AS auto) between methods of $\overline{\Delta\kappa_r} = 0.0013$ s and standard deviation of $\sigma(\Delta\kappa_r) = 0.0078$ s. On the other hand, the correspondence of measured values is poor in the case of HASLI (the worst case), with an average difference over ten times larger at $\overline{\Delta\kappa_r} = 0.018$ s and a standard deviation of $\sigma(\Delta\kappa_r) = 0.017$ s. For the other stations, the comparison is generally acceptable: BALST $\Delta\kappa_r = 0.0056 \pm 0.0089$ s; PLONS $\Delta\kappa_r = 0.0088 \pm 0.0130$ s; SULZ $\Delta\kappa_r = 0.0076 \pm 0.0095$ s and BNALP $\Delta\kappa_r = 0.0100 \pm 0.0140$ s. The average differences can be interpreted as relative bias between the methods, while the standard deviation indicates the 'robustness' of measurements.

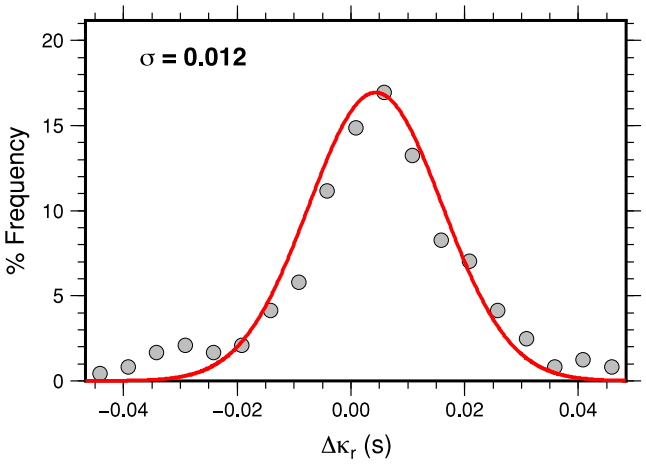

Figure 4. Frequency distribution of $\Delta\kappa_r$ at site LLS between the manual AS approach and the station specific BB approach (κ_rAS-κ_rBB). The red line shows a best-fitting normal distribution with standard deviation 0.012 s. A normal distribution could not be fit to the log-space residuals [i.e. $\ln(\kappa_r\text{AS}/\kappa_r\text{BB})$].

4.2 Suitability of the κ_r attenuation model

The poor correspondence of measured κ_r between the automatic and manual approaches at site HASLI is interesting and deserved further investigation, since it would significantly change the κ_0 determined for this site. The reason for the difference was found to be related to a curvature (Fig. 6) of the high-frequency part of the acceleration spectrum in lin-log space. The FAS is assumed to be linear for the standard κ_r model to work (assuming frequency-independent Q within the range of frequencies used), and in that case the choice of frequency range (f_1 and f_2) to be fit within the linear part should not make a difference. For a curved FAS, however, the choice of f_1 and f_2 is mapped into the measured κ_r. While the automatic approach tends to use a similar value of f_1 (10 Hz, unless the SNR restricts this) and as high as possible a value of f_2, the manual approach tended to favour picking lower values of f_1, where the spectrum was decaying faster, and restricting f_2 to lower values so as not to allow bilinear trends in the spectral decay (Fig. 6).

One explanation for the curved spectrum decay in log-lin space is the frequency dependence of Q. For instance, attenuation using a frequency-dependent Q [e.g. $Q(f) = Q_0 f^\alpha$] could be modelled, similarly to the standard κ_r model, as an exponential with $\exp(-\pi f^{1-\alpha} \kappa_r)$. If the spectrum were then plotted in lin-log space,

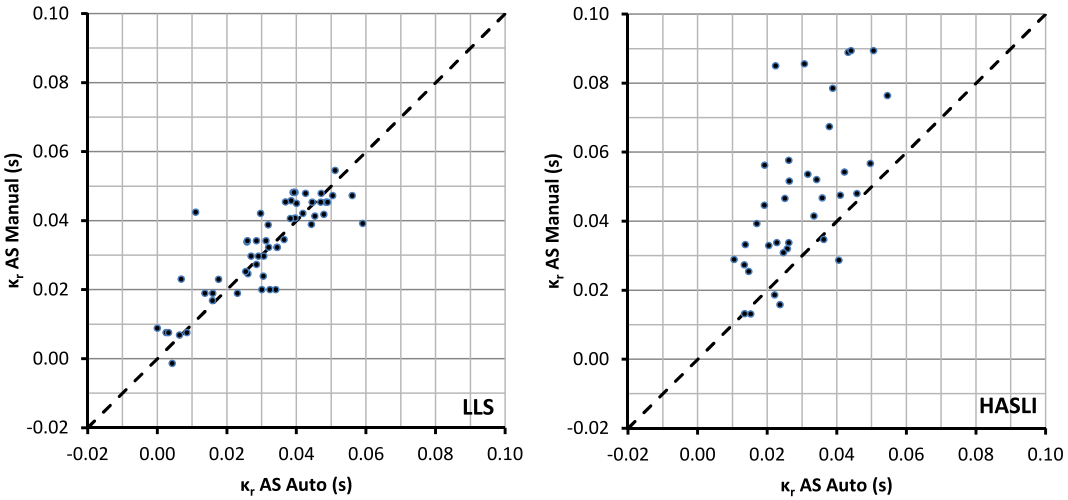

Figure 5. Comparison of κ_r using the manual and automatic high-frequency (AS) fitting approaches at stations LLS (best case) and HASLI (worst case).

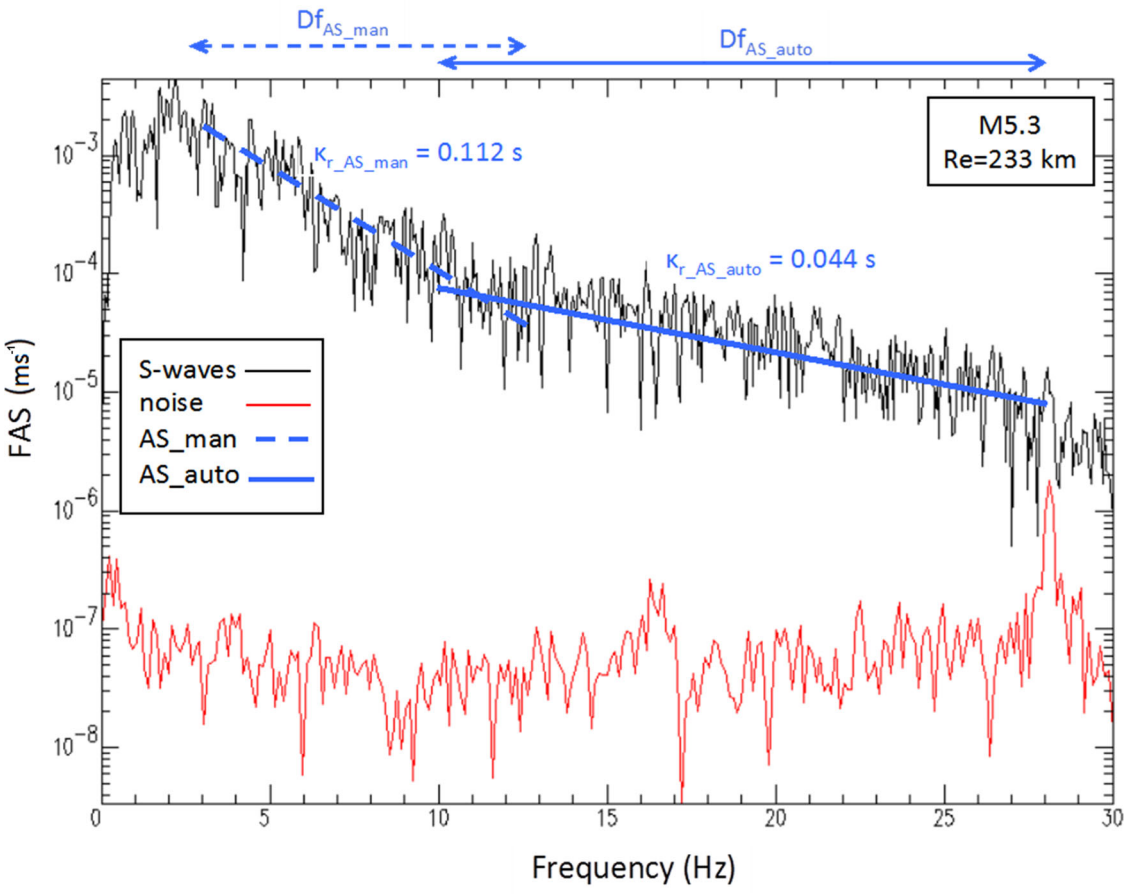

Figure 6. Example of spectral decay observed at site HASLI for the acceleration FAS (black) compared to the noise FAS (red). The dashed blue line indicates the fit of the AS manual approach while the continuous blue line indicates the fit of the AS auto approach. The difference in the two is due to the nonlinear shape of the decay.

then this would lead to a curved decay over high frequencies, with decreasing decay at higher frequencies (assuming $\alpha > 0$). Frequency dependent attenuation over the frequency band analysed here is certainly possible in Switzerland, and is also typically seen in other regions (e.g. Atkinson & Mereu 1992; Raoof *et al.* 1999). For instance Goertz-Allmann & Edwards (2014) found that a models with the form $Q(f) = 467f^{0.3}$ and $Q(f) = 260f^{0.34}$ were appropriate for modelling a Swiss regional data set using two spectral fitting methods. Previously Bay *et al.* (2005) found Q_0 to range from 220 to 440 and α to vary correspondingly from 0.56 to 0.37 in Switzerland for different assumed geometrical decay models.

Another reason behind the curvature may be the amplification behaviour as site HASLI, which starts to increase almost linearly in the high-frequency range starting at 10 Hz (Fig. 2), an issue that is

investigated in more detail in the section '4.5 effect of near-surface amplification'. Regardless of the reason, in the case that our observed data do not conform to the Anderson & Hough (1984) κ_r model (i.e. the assumptions of frequency-independent Q and flat amplification in the high-frequency range), then significant differences will arise depending on the fitting choices. In the case of station HASLI, the automatic approach tends to fit the decay at higher frequencies ($f > 10$ Hz), while the manual approach favours fitting the higher decay in the middle of the spectra ($3 \lesssim f \lesssim 15$ Hz) (Fig. 6). Ultimately, there is no explicitly correct choice, since the underlying high-frequency linear decay model does not hold. The degree of linearity of the high frequency decay, and therefore conformity to the κ_r attenuation model, is a clear source of epistemic uncertainty. The fact that different methods tend to fit different frequency ranges then manifests as systematic bias. Nevertheless, the use of different κ_r estimation approaches can help to represent this epistemic uncertainty. Furthermore, in the case of seismic hazard estimation or engineering applications, where response spectral ordinates are required, the impact of high-frequency ground motion on oscillator response rapidly diminishes. Short oscillator periods (e.g. < 0.1 s) are sensitive to longer period ground-motion, so it would be preferable to choose methods that focus on the lower frequency end of the linear decay.

In order to explore this source of epistemic uncertainty further we systematically compare the shape of the high frequency decay for our six rock sites. First all spectra from events with $M_L \geq 3.5$ at a particular site were corrected for κ_r determined using the AS auto approach; the spectral amplitudes were then normalized to unity at 10 Hz and stacked (Fig. 7). It should be noted that different interpretations can be made depending on the choice of normalization frequency. Nevertheless, the choice of 10 Hz is conservatively high: many analyses would extend to even lower frequencies to measure kappa, so it would be difficult to justify increasing the frequency (e.g. to 15 Hz such that the trend at BALST is flat). At low frequencies ($f < 5$–10 Hz), a deviation from the linearity should be present due to the source corner-frequency of the records: this will show as a deviation to values less than 1. For a perfectly linear decay (above the low frequency range) conforming to the κ_r AS auto value, the mean (and median) normalized spectra in Fig. 7 should follow a straight line with constant amplitude. In the case that the κ_r model is appropriate, but the correction using κ_r AS auto is inadequate, then a linear gradient will exist. Finally, in the case that the line is not straight in the high-frequency part, then the κ_r decay model is not valid for this data. For instance, station LLS, where the best match between fitting methods was present, shows a broadly linear decay from 8 to 30 Hz (evident as a constant value of normalized acceleration in Fig. 7), with the source corner frequency effect showing below 8 Hz. On the other hand, for station HASLI, we observe the bi-linear decay also seen in Fig. 6, with stronger linear decay from 7 to 12 Hz then weaker linear decay from 12 to 30 Hz. In this case the correction for κ_r AS auto (measured for 10–30 Hz) provides an 'average' of the two decay slopes. The manual approach, as previously noted, focussed on the higher decay section, leading to higher estimates of κ_r (Fig. 6). Station PLONS and, to a lesser extent, station BNALP also seem to suffer from this curved or bi-linear decay effect. These effects are likely to be related to the frequency dependence of Q that is not considered using the approach of (Anderson & Hough 1984) or the implemented broad-band approach. Station

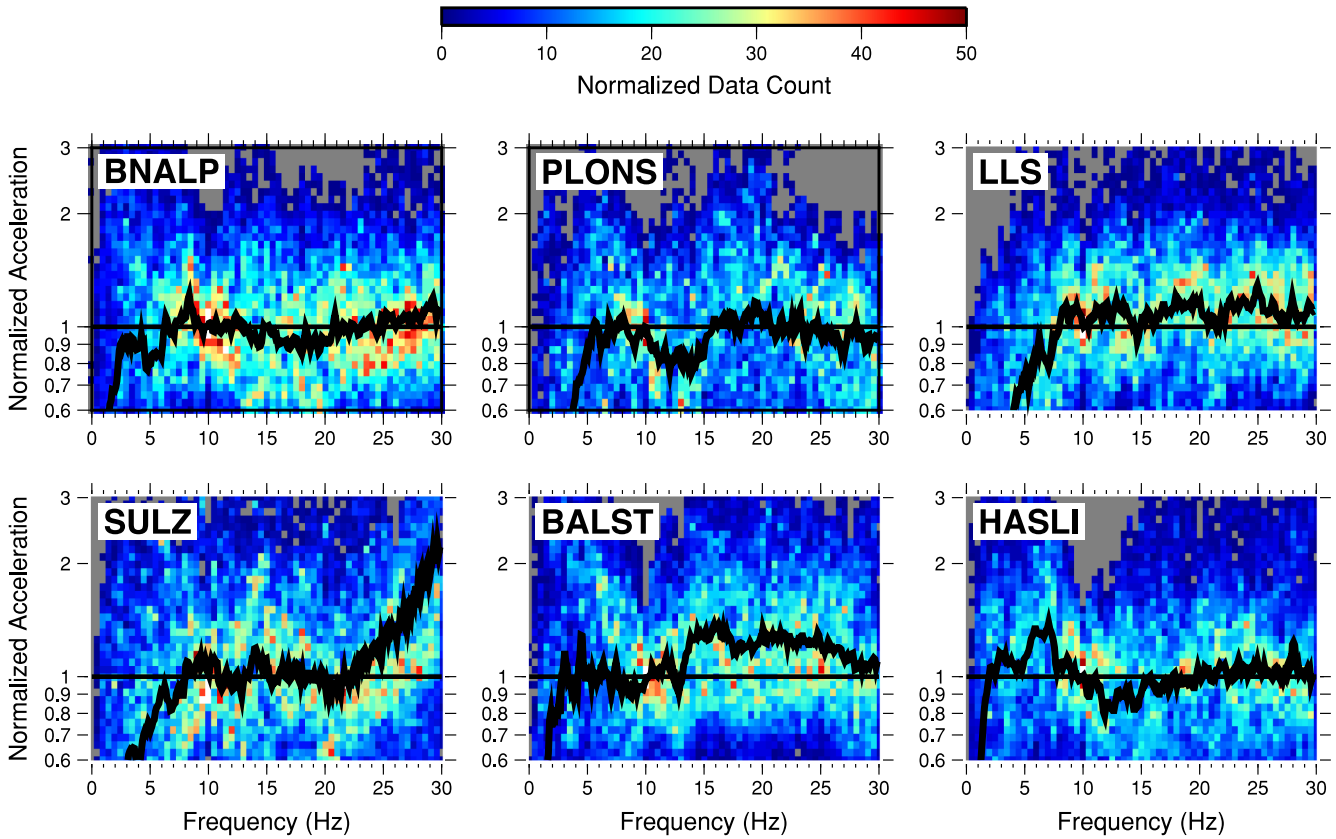

Figure 7. Plots highlighting the linearity of high-frequency spectral decay at each of the stations. Normalized acceleration spectra are stacked after being normalized by a single record-specific decay (κ_r from AS auto) and by the spectral value at 10 Hz. The black lines indicate the log-mean. Linear decay in the FAS should be seen as a straight line with unit amplitude.

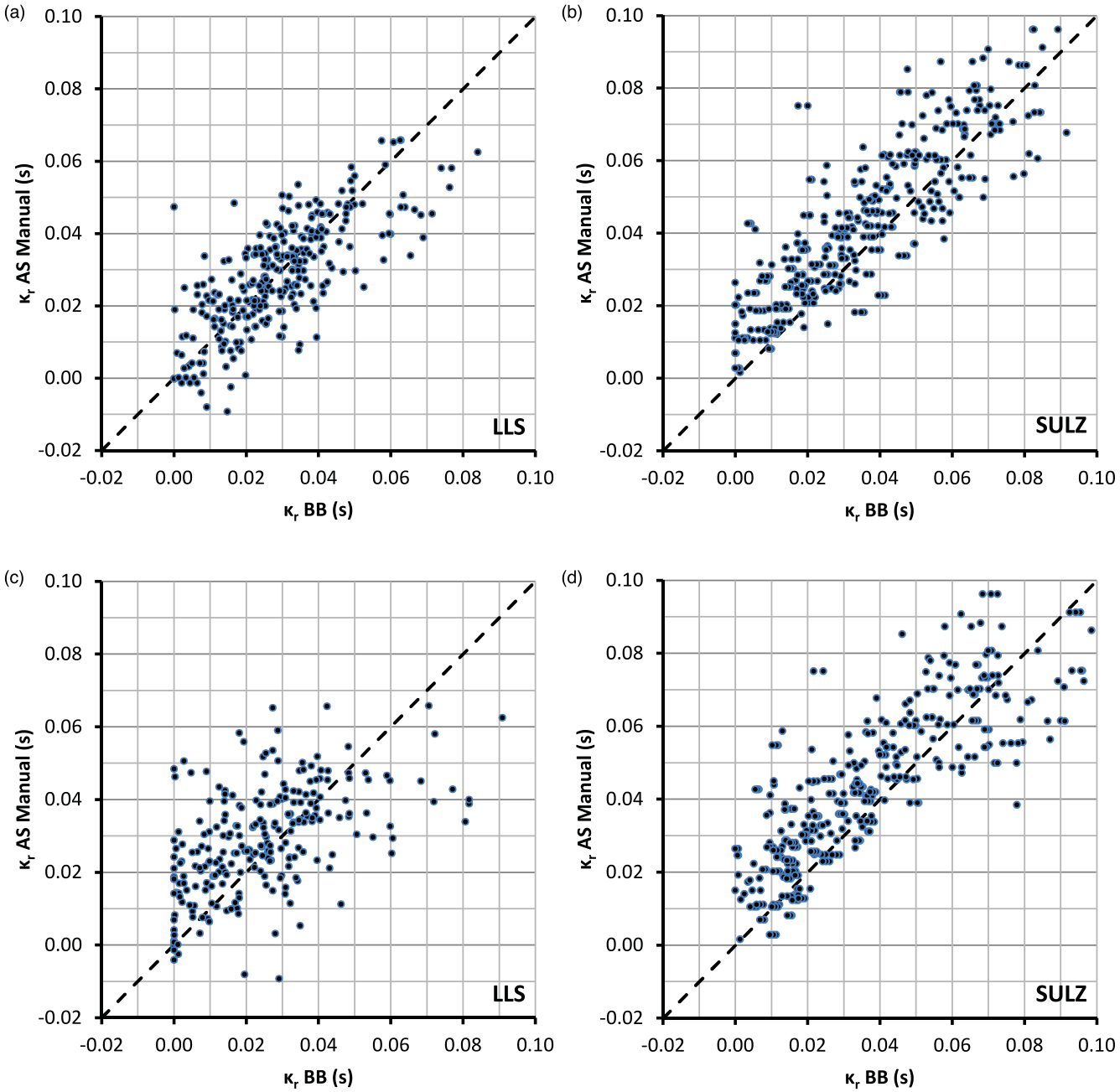

Figure 8. Comparison of broad-band κ_r estimates with manual high-frequency estimates for stations LLS and SULZ. (a, b) using station-specific apparent f_c; and (c, d) using event-specific f_c.

BALST clearly shows the effect of amplification (Fig. 2), which will also lead to different κ_r measurements, depending on the fitting range. Beyond 20 Hz station SULZ shows a weaker decay from the measured κ_r AS auto, although this would likely be misinterpreted as noise—with a flattening out of the FAS beyond 20 Hz.

4.3 Comparison of κ_r BB approaches

We next compare estimates of measured κ_r from the broad-band approaches [using (1) event-specific f_c and (2) station-specific apparent f_c], κ_r BB, with those from the manual high-frequency fitting approach, κ_r AS. This comparison (Fig. 8) includes about four times more data, since all approaches used small earthquakes (down to $M_L = 2$). For the broad-band approach with station-specific apparent f_c, the match tends to be more consistent than for the approach with event specific f_c. Using the station specific f_c we obtain a lower standard deviation in the differences between κ_r AS and κ_r BB compared to using the event-specific f_c approach. This is expected, since in the station-specific apparent f_c approach we aim simply to fit the spectral shape as best as possible (similarly to the high-frequency AS approach). This may be due to the fact that any potential frequency dependence of Q can somehow be accommodated by a distance dependent f_c. On the other hand, in the event-specific f_c approach there are fewer degrees of freedom, aiming to stabilise the inversion and obtain a source-specific stress-drop consistent with a single source corner-frequency. For LLS we note that there is negligible offset between the broadband and manual high-frequency

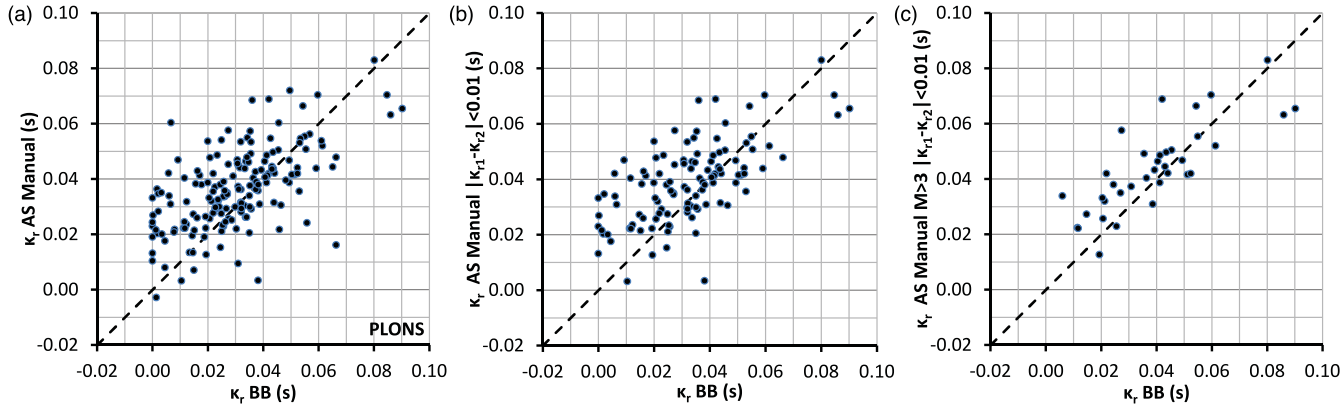

Figure 9. Comparison of broad-band κ_r estimates with manual high-frequency estimates for station PLONS. (a) all data; (b) data where the two horizontal component estimates of κ are less than 0.01 s apart for the manual approach; (c) as (b), but also only data from events with $M_L > 3$.

estimates, however, for SULZ the broad-band fit tends to lead to slightly lower values.

In Fig. 9 we show the effect of introducing stricter κ_r selection criteria into the comparison. Station PLONS shows an average standard deviation between the measured values, but this decreases when we include only κ_r measures that are within 0.01 s on each horizontal component. The standard deviation between the measured values decreases further when comparing only events with $M_L > 3$. There are several reasons for this: larger events are less susceptible to the trade-off between f_c and κ_r, include more bandwidth between f_c and the highest usable frequency (i.e. maximising the range $\Delta f = f_2 - f_1$ over which κ_r is measured), are generally less noisy and have more points in the FFT that can be used.

4.4 Summary of κ_r estimation approaches

An overview of the measurement offset and standard deviation between κ_r determined using different methods is given in Table 1. It is immediately apparent that the manual AS approach consistently leads to higher estimates, with all $\Delta\kappa_r$ but one in Table 1 being negative. The largest average systematic difference is actually between the manual and automatic high-frequency AS approaches (0.018 s), highlighting that the choice of the fitting bandwidth (f_1 and f_2) is a significant source of uncertainty. For the broad-band approaches the average measurement difference is slightly greater for the event-specific f_c approach at some sites. The standard deviation of the measurement differences, giving an indication of our measurement and modelling error, is rather high for all approaches, with averages over all six sites of between 0.012 and 0.017 s. This error is large considering that typical values of κ_r are of the order of ten to hundreds of ms, depending on the site and recording distance. Given the simplistic and empirical nature of the κ_r parameter, it is difficult to choose the more 'correct' κ_r model. Instead, this result highlights the importance of retaining consistency between the derivation process for κ_r (and subsequently κ_0) and any forward applications (e.g. stochastic simulation, site response analyses).

4.5 Effect of near-surface amplification

Within a particular method, the largest differences and standard deviations in measured κ_r tend to be for those sites known to exhibit site amplification effects, albeit limited, in the range 10–30 Hz (Fig. 2): in particular BALST and HASLI. Sites exhibiting amplification in this range will be more sensitive to the choice of the fitting limits (f_1 and f_2), particularly using the high-frequency AS approaches. For instance, Parolai & Bindi (2004) observed the possible bias that may be introduced on the measurement of κ_r due to resonant peaks distorting the spectral shape, which is otherwise assumed flat. Furthermore, crustal amplification also has an influence on the spectral shape at high frequencies (Boore & Joyner 1997). However, Poggi *et al.* (2011) showed that crustal amplification for Switzerland can be considered flat above around 5 Hz.

In order to test the effect of near-surface amplification on measured κ_r at sites BALST and HASLI, we computed the theoretical effect of the shape of the amplification function on the measurement, as a function of the lower and upper fitting frequency limits (f_1 and f_2). Specifically we measure the average gradient of the amplification function between the limits f_1 and f_2 (Fig. 2), as shown in the lower part of Fig. 10. Since κ_r is measured from the gradient of the FAS at high frequency, the additional gradient due to the amplification function manifests as a change in the measured κ_r, termed $\Delta\kappa_{r,AMP}$. Effectively $\Delta\kappa_{r,AMP}$ reflects the bias on the κ_r measurement due to the 'distortion' of the FAS shape by amplification. The measurement of $\Delta\kappa_{r,AMP}$ is performed on moving windows: we

Table 1. Mean offset and standard deviation of κ compared to the high-frequency AS manual approach.

Station	Vs_{30} (m s^{-1})	Site effects (10–30 Hz)	BB (station f_c) $\Delta\kappa_r$ (s) Mean	σ	BB (event f_c) $\Delta\kappa_r$ (s) Mean	σ	AS (auto) $\Delta\kappa_r$ (s) Mean	σ
LLS	3000	No	0.001	0.011	−0.004	0.016	−0.001	0.008
HASLI	1600	Yes	**−0.010**	**0.020**	*−0.005*	**0.021**	**−0.018**	**0.018**
BNALP	1650	No	−0.006	0.013	−0.006	0.017	−0.010	0.014
PLONS	1810	Slight	−0.006	0.015	−0.007	0.016	−0.009	0.013
SULZ	1030	No	−0.007	0.015	−0.006	0.015	−0.008	0.010
BALST	1350	Yes	−0.006	0.016	**−0.012**	*0.015*	−0.006	0.009
Average			−0.006	0.015	−0.007	0.017	−0.009	0.012

Note: Values in italics show the largest differences, while those in bold are the highest per category.

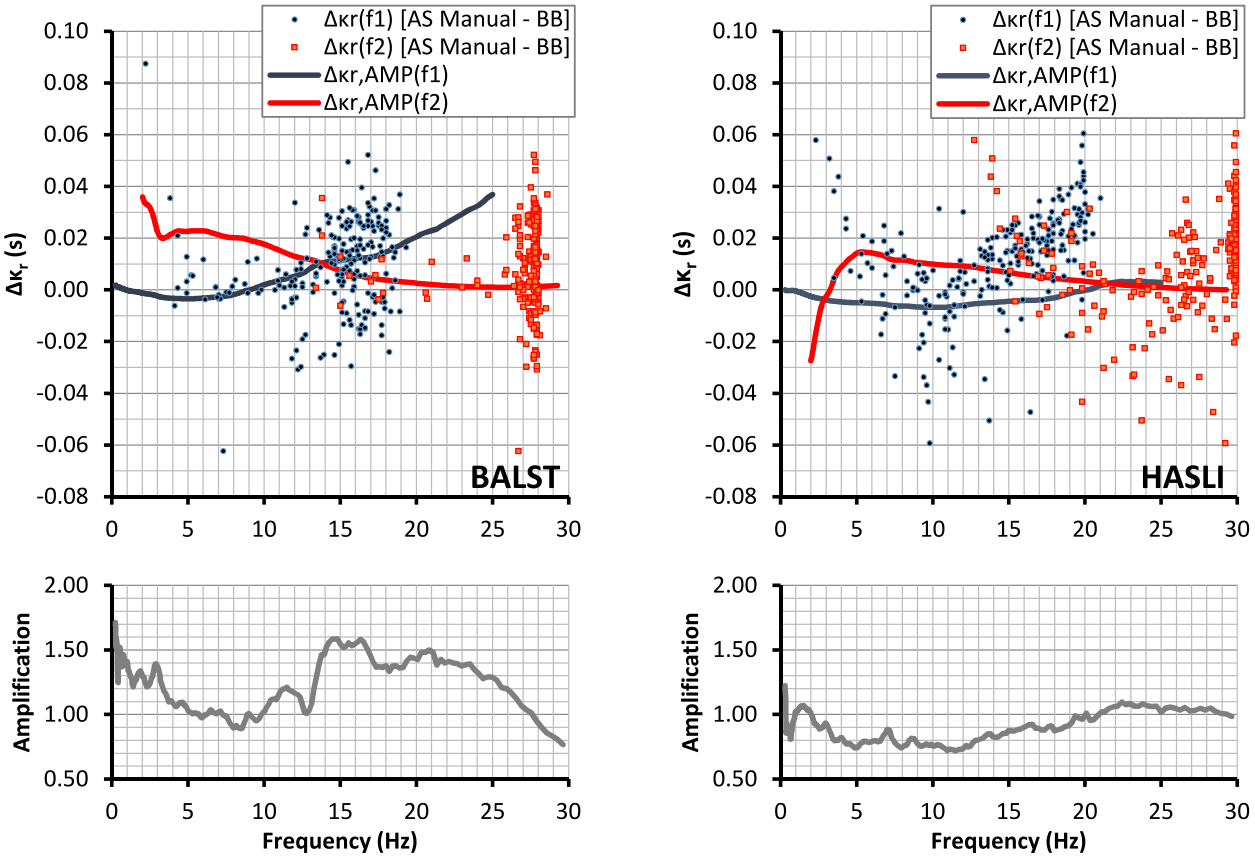

Figure 10. Difference in measured κ_r [$\Delta\kappa_r$ = AS (manual) – BB (station specific f_c)] at site BALST and HASLI as a function of the fitting bandwidth (lower limit: f_1 and upper limit: f_2). Lines in the upper panels show the corresponding theoretical $\Delta\kappa_{r,AMP}$ due to amplification (lower panel).

keep one edge constant (fixed at the lowest or highest frequency respectively) and move the other. For example, in computing the effect of the choice of f_1 on $\Delta\kappa_{r,AMP}$, we fix f_2 to 30 Hz, and when assessing the effect of f_2 we fix f_1 to 0.2 Hz. Note here that the source corner frequency, which would also significantly affect measured κ_r if ignored, is not considered in this test since we focus only on the effect of amplification. The computed bias due to varying f_1 or f_2 is shown in Fig. 10. In the same figure we plot an estimate of the observed bias: represented by the difference between the broad-band and high-frequency approaches. Whilst there is significant scatter, the differences in measured κ_r follow the expected effects due to the influence of amplification on the high-frequency fitting method for site BALST. For HASLI, the general trend of the theoretical $\Delta\kappa_{r,AMP}$ versus f_1 and f_2 is present in the measured $\Delta\kappa_r$ values, but it is not as clear. This suggests an additional influence on the measurement differences than amplification alone. Furthermore, the theoretical differences in measured κ_r due to amplification, within reasonable bounds (e.g. f_2 as low as 10 Hz or f_1 as high as 20 Hz), lead to $\Delta\kappa_{r,AMP}$ of up to 20 ms, even for these 'hard-rock sites' with limited amplification. Actual observed differences are as much as 60 ms, which is clearly not attributable to the amplification effects alone. Possibly this is due to the non-linearity of the high-frequency decay due to frequency dependent Q or some other systematic departure from a linear high-frequency decay (Figs 6 and 7).

5 MODELLING Q AND κ_0

The previous analyses focussed on uncertainties related to the measurement of individual κ_r values. They indicate that, depending on the choice of method and even the specifics of one method, differences in the estimated κ_r can be large. For seismic hazard, when using for example, the point source stochastic model, we typically model attenuation by choosing correlated sets of parameters (Q, geometric spreading, κ_0, stress drop). The total attenuation due to Q and κ_0 is then modelled as:

$$\kappa_r = t^* = \frac{R}{\beta Q} + \kappa_0, \quad (1)$$

where $\kappa_r = t^*$ is the whole-path attenuation term, β is the average shear-wave velocity in the crust, Q describes the crustal attenuation, assuming it is frequency-independent and R is some source-site distance metric (e.g. epicentral or hypocentral distance). Originally κ_r was defined using epicentral distance, however, either distance may arguably be implemented as long as consistency is retained for subsequent forward-modelling (e.g. stochastic simulation of acceleration time-series). κ_0, as discussed previously, is assumed to be a site-specific attenuation term and is therefore particularly useful for site-specific spectrum adjustments. Clearly, due to the variability and method bias in κ_r, estimation of both Q and κ_0 will be subject to significant uncertainty and potential bias.

The determination of Q and κ_0 is analogous to determining the gradient and intercept of a straight line fitted to the κ_r measurements at one station versus distance. Data selection will clearly have an influence on the resulting parameters: we aim to balance selecting sufficient, but high-quality data. The robustness of the regression can be further increased by initially determining a crustal Q that is applicable to all stations at the cost of increase in the misfit; meaning we only need to search for the intercept.

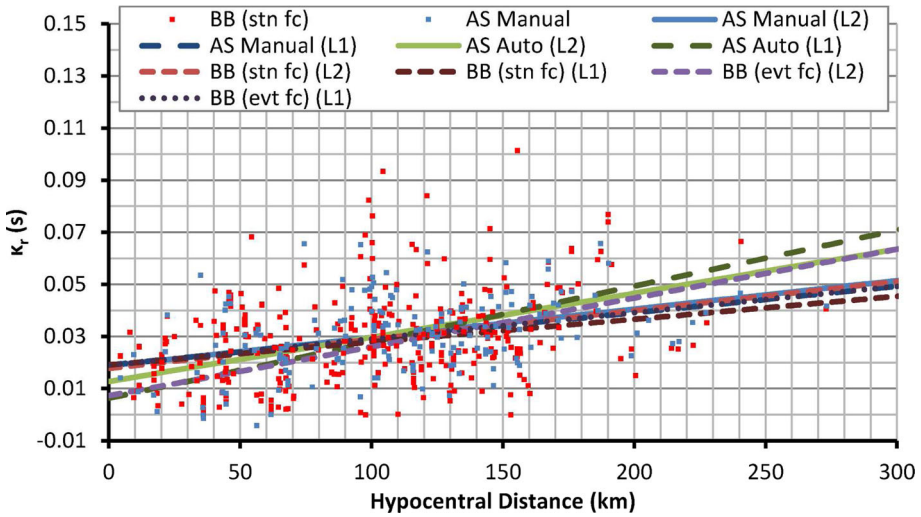

Figure 11. Comparison of the different Q and κ_0 models for a single station LLS. For reference two data sets are plotted: 'BB(stn fc)' are the data from the broad-band method (with station specific f_c), 'AS manual' are the data from the manual high-frequency approach. The models are for different fit types ('L1' – absolute amplitude; 'L2' – least-squares) and for different origin data sets: 'BB' indicates broad-band methods, 'AS' indicates high-frequency methods, as discussed in the text.

5.1 Effect of κ_r estimation method and regression type on Q and κ_0

Station LLS represented the best-case scenario for determination of κ_r, with all methods apart from the broad-band event-specific f_c approach showing comparatively low mean and standard deviation between methods ($\Delta\kappa_r$). Nevertheless, deriving Q and κ_0 for even this case is not straightforward. Across the different κ_r data sets (AS auto: high-frequency automatic fit; AS manual: high-frequency manual fit; BB (station f_c): broad-band station-specific source corner frequency; and BB (event f_c): broad-band event-specific source corner frequency) and two different fitting methods (L1: absolute amplitude; L2: least-squares) we obtain eight possible models (Fig. 11, Table 2). In addition, we tested using R_{epi} instead of R_{hyp} for the AS (manual) fit κ_r data, but the difference was negligible (as expected considering the wide distribution of distances). The use of epicentral or hypocentral distance is only an issue for stations where many near-source recordings are dominant, which is rare. The differences arising from different fitting methods (L1 or L2 norms) were generally small, but not necessarily negligible: in the case that outliers are expected, L1 or similar outlier-resistant solutions (e.g. the weighted robust regression used in Ktenidou *et al.* 2013) might therefore be preferred. The differences due to the method used to derive the input data κ_r are by far the most significant: for station LLS, κ_0 ranges between 0.007 and 0.019 s.

Despite the similarity in the average κ_r derived for station LLS (Table 1), the large scatter relative to our chosen model (eq. 1) means that the data selection and Q– κ_0 regression type heavily impacts the resulting Q and κ_0. This is further exemplified using a bootstrap analysis of the high-frequency AS (manual) κ_r: 1000 subsamples with repetition were made of this data set, and each one was used to determine the model parameters (Fig. 12). The resulting 95 per cent confidence interval for κ_0 was between 0.0136 and 0.0237 s while the 95 per cent confidence limit for Q ranged from 1926 to 3934. This variability can therefore help to explain

Table 2. Different Q_0 and κ_0 models for station LLS.

	L2 (data-driven Q)				L1 (data-driven Q)				L2 (fixed Q)		
	Q	Q 68 per cent limits	κ_0 (s)	$\sigma(\kappa_0)$ (s)	Q	Q 68 per cent limits	κ_0 (s)	$\sigma(\kappa_0)$ (s)	Q	κ_0 (s)	$\sigma(\kappa_0)$ (s)
AS Manual R_{epi}	2606	2207–2748	0.0188	0.0026	2838	2237–3074	0.0191	0.0035	1200	0.0045	0.0011
AS Manual R_{hyp}	2621	2494–2762	0.0187	0.0026	2834	2632–3068	0.0190	0.0035	1200	0.0043	0.0011
AS Auto R_{hyp}	1690	1624–1761	0.0128	0.0030	1328	1251–1415	0.0063	0.0057	1200	0.0051	0.0013
BB (Stn f_c) R_{hyp}	2573	2481–2672	0.0178	0.0015	3253	3059–3473	0.0191	0.0021	1200	0.0050	0.0007
BB (Evt f_c) R_{hyp}	1523	1477–1572	0.0073	0.0027	2834	2623–3082	0.0190	0.0037	1200	0.0021	0.0011

Table 3. Selection criteria for determination of κ_0 from κ_r AS measurements. The bold criteria were adopted for this study.

Set of criteria	Quality criteria for selecting κ_r AS measurements	Per cent of total data used
1	No criteria (all κ are taken)	100
2	$df > 8$ Hz	98
3	$df > 8$ Hz; $\kappa > 0$	95
4	$df > 8$ Hz; $\kappa > 0$; $\Delta\kappa < 50$ per cent	78
5	$df > 8$ Hz; $\kappa > 0$; $\Delta\kappa < 50$ per cent; $M > 2.5$	45
6	**$df > 8$ Hz; $M > 2.5$**	55
7	$df > 8$ Hz; $M > 3$	24

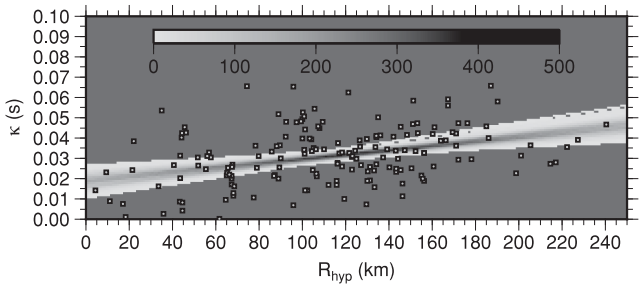

Figure 12. Bootstrap analysis of the H_f Manual κ_r data (squares) using the L2 fit for site LLS. The scale indicates the number of solutions represented by any one point.

the significant method-to-method differences in parameter values. This large variability also indicates that we need a sufficiently large data set to constrain the mean, and that working with a small data set can lead to bias.

5.2 Effect of κ_r selection and assumption of Q on κ_0

We make another sensitivity analysis to see how the choice of data affects the computed slope and intercept. Different sets of quality criteria (Table 3, Fig. 13, top) are defined, with different levels of strictness, in order to choose subsets of κ_r values from our data. We use the κ_r values from the seven subsets, allowing for data-driven determination of Q. An example of the results in terms of κ_0 and Q is shown in Fig. 13 (bottom). To strike the balance between good quality data and sufficient volume, we choose criteria no. 6 (Table 3, $\Delta f > 8$ Hz and $M > 2.5$). The following analyses are therefore performed with this set of criteria.

An approach often taken to improve the robustness of κ_0 determination is to fix or constrain Q. This may either be in the form of taking a value from the literature, or by including all stations in a combined inversion for a common, region-specific Q and station-specific κ_0. Using a value of $Q = 1200$, as used by Edwards & Fäh (2013b) for Switzerland, we repeated the analysis for station LLS using the L2 fit (Table 2). In this case the κ_0 values are indeed more similar between the methods, but the value is lower than using the station-specific Q. We then used the AS manual fit to obtain a common regional Q and site-specific κ_0. This resulted in $Q = 1948$, across the six selected sites in this study and $\kappa_0 = 0.0145$ s for site LLS (Fig. 14, Table 4). It is clear therefore, that while fixing or constraining Q results in more robust κ_0 between methods, the choice of Q then significantly affects the results. The two values used here (1200 and 1948) correspond to different background data sets: the former being the average over 83 Swiss stations, including strong-motion sites, while the latter is from only the six stations in this study. Looking at available Q studies in the literature, our data-driven Q value is near what Drouet *et al.* (2010) found for the Rhein Graben, for the frequency range of measurement, which is roughly 15–30 Hz. The fixed value of 1200 is in line—over the same frequency range—with the results of Bay *et al.* (2003) for Switzerland, while between these two estimates lie the results of Douglas *et al.* (2010) for France.

In Fig. 14, aside from the mean estimates of κ_0 per station, we also show the standard error of the mean and the standard deviation of the data points within the first 100 km. The former is rather low, implying high confidence in the mean for a particular data set, while the latter is rather high (e.g. ten times higher), implying that we need a large number of records—over 100 at most stations—to

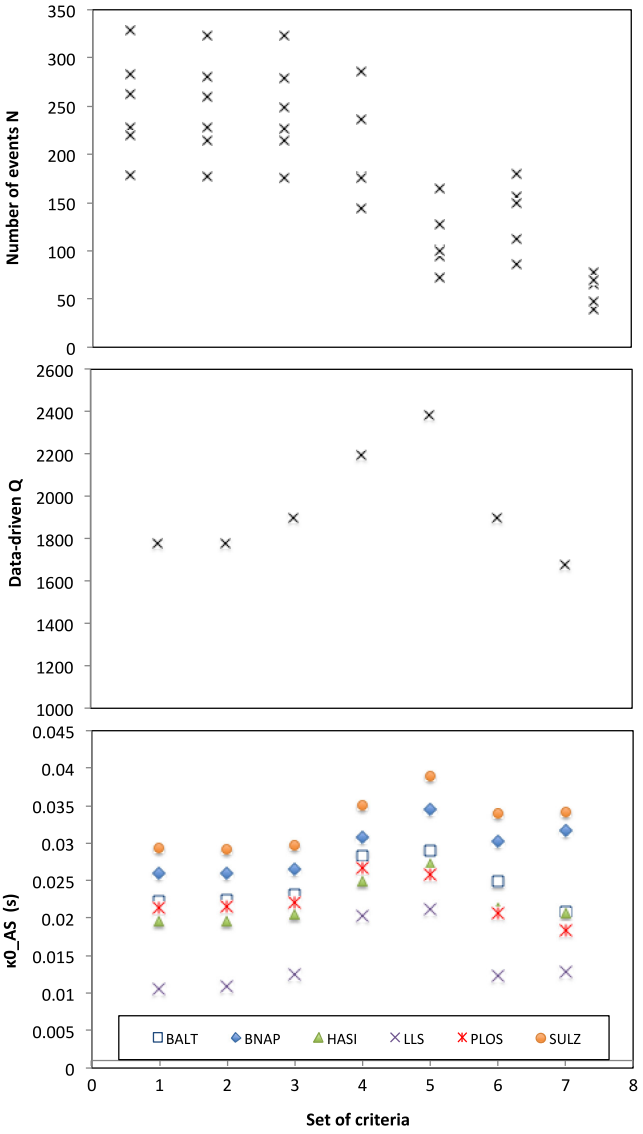

Figure 13. The definition of the quality criteria sets (Table 3) used to select κ_r values from the AS manual method and the variability in the number of data, Q and κ_0 (bottom) when applying them.

get a reliable estimate of the mean κ_0 value. At most sites where we need to characterize κ_0, we do not have such a large volume of data. This means that it may be difficult in the presence of few records to get a reliable estimate of the mean value.

5.3 Epistemic uncertainty of κ_0

A summary of κ_0 and corresponding Q values for all six hard-rock stations is shown in Table 4. One could consider this range of κ_0 and Q values to reflect the uncertainty due to modelling choices (a source of epistemic uncertainty). If each of the 20 κ_0 values is assumed to be equally technically defensible and have an equal probability of representing the true κ_0 model, then we can quantify the epistemic uncertainty of κ_0 related to modelling approaches using the standard deviation and corresponding confidence interval. Assuming a normal distribution, the epistemic standard deviation at each station is shown in Table 4. A quantile–quantile plot is shown in Fig. 15 showing the conformity of the κ_0 values to either a normal or log-normal distribution. Neither provides perfect conformity, but

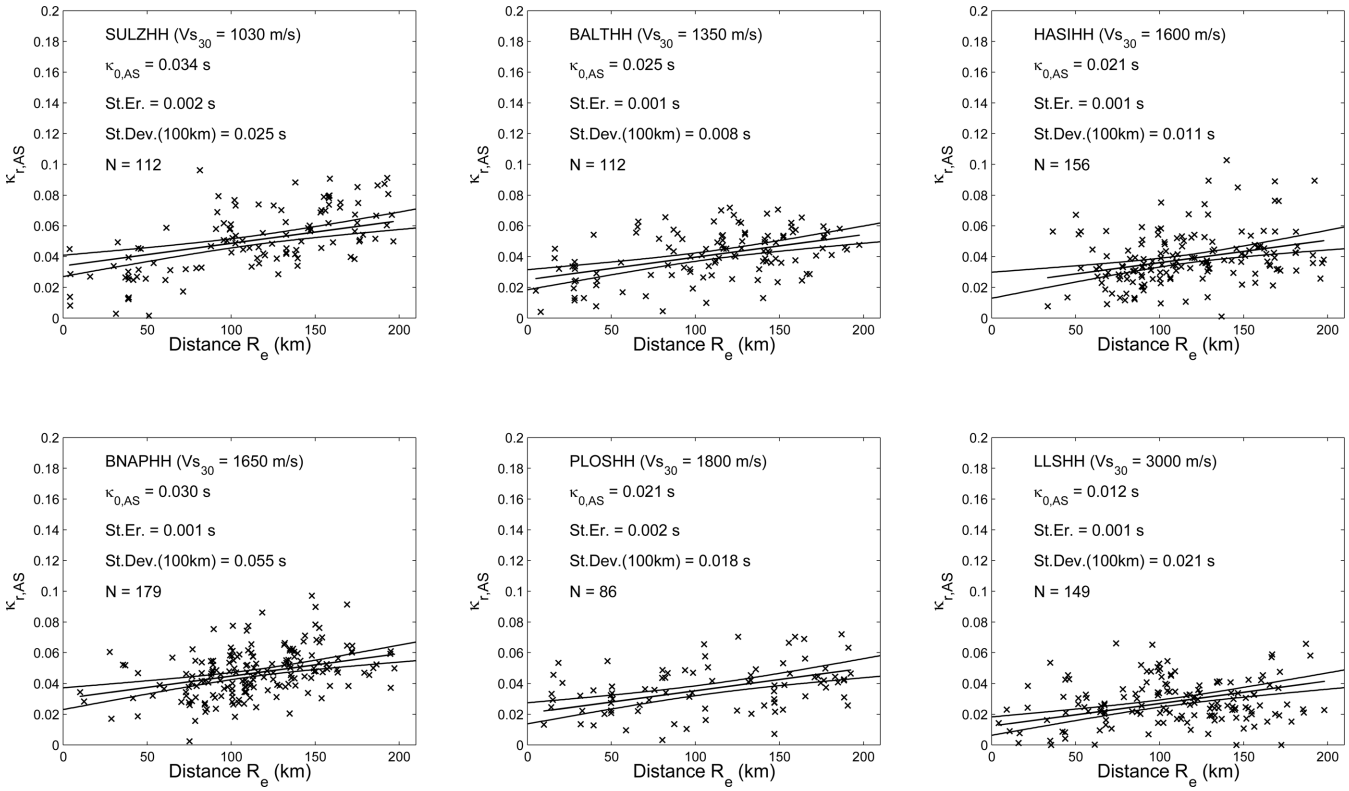

Figure 14. Determination of a common Q and regression for site-specific κ_0 values using the AS manual fit κ_r data. These regressions were performed for the set of criteria #6 ($df > 8$ Hz and $M > 2.5$). They yield a common region-specific Q of 1948. The results include the mean and the 95 per cent confidence interval accounting for the uncertainty in both intercept and slope. We note the values of the mean κ_0, its standard error, and the standard deviation σ for data points out to 100 km. Station labels: BALST (BALT); BNALP (BNAP); HASLI (HASI); PLOS (PLONS); LLS (LLS); SULZ (SULZ).

a normal distribution is closer to the observed distribution, with better behaviour in the tails of the distribution. The average standard deviation of κ_0 from the different approaches is 0.0083 ± 0.0014 s. Station LLS showed a lower epistemic uncertainty, with a standard deviation of 0.0062 s. This is consistent with the observations that it had the most limited amplification of all sites, and that the spectral decay was completely linear beyond around 8 Hz (Fig. 7). For the other stations, significant deviations from the linear-decay, in some cases obviously produced by amplification phenomena, leads to higher uncertainty.

6 RELATION OF Vs_{30} to κ_0

Assuming that κ_0 is a property of the site, it is useful to compare the κ_0 results of this study with other shallow geotechnical characteristics, as this may provide proxies to predict κ_0 in the absence of recorded data. One of the most commonly used site classification metrics is Vs_{30}, indicating the travel-time average shear-wave velocity of the upper 30 m of soil or rock. Several authors have presented empirical Vs_{30}-κ_0 correlations based on different data sets (e.g. Silva *et al.* 1998; Chandler *et al.* 2006; Drouet *et al.* 2010; Edwards *et al.* 2011; Van Houtte *et al.* 2011; Edwards & Fäh 2013a; Poggi *et al.* 2013), each showing that between low and moderate Vs_{30} a loose correlation exists; with κ_0 decreasing with increasing Vs_{30}. However, at high Vs_{30} values ($Vs_{30} > 1000$ m s^{-1}) it is not clear if such a trend continues.

Authors typically use only one method to compute the κ_0. Consequently, as shown in the previous analyses, we might expect significant differences between the studies, with additional uncertainty due to the limited number of data and the fact that they come from different regions (Ktenidou *et al.* 2014). In Fig. 16, several existing Vs_{30}-κ_0 correlations are compared to the range of values determined in this study. The selected range of Vs_{30}–κ_0 correlations covers both broad-band and high-frequency approaches (both automatic and manual). Vs_{30}–κ_0 correlations are generally very simple models (e.g. linear or log-linear regressions), which indicate decreasing κ_0 with increasing Vs_{30}, even above 1500 m s^{-1}. Our results show that such trends are not possible to statistically justify. At least part of the sources of epistemic uncertainty can be qualified through comparing the κ_0 resulting from the different approaches (AS and BB) and different Q (free, 1200 and 1948) assumptions (Fig. 16). It is clear that the average BB solutions are lower than the AS solutions, with the ranges only barely overlapping at some stations (e.g. at SULZ). However, the Q assumption also strongly, and systematically, influences the κ_0 values. In this sense, it cannot be suggested to focus on either method or Q sources in order to reduce the uncertainty, rather both should be jointly investigated.

Hashash *et al.* (2014) recommended a reference rock ($Vs_{30} = 3000$ m s^{-1}) κ_0 for central and eastern North America of 0.006 s, with standard deviation in $\ln(\kappa_0)$ of 0.43. The latter was partly based on the range of measured hard-rock κ_0 in central and eastern North America. The average κ_0 for site LLS (also with $Vs_{30} = 3000$ m s^{-1}) lies within two standard-deviations of the Hashash *et al.* (2014) reference rock κ_0 model. All measured κ_0 (here representing our epistemic uncertainty) for site LLS lie within their three standard-deviation range.

Table 4. Summary of κ_0 determined for the six hard-rock stations and corresponding Q.

	Method	LLS		BNALP		PLONS		HASLI		BALST		SULZ	
		κ_0 (s)	Q	κ_0 (s)	Q	κ_0 (s)	Q	κ_0 (s)	Q	κ_0 (s)	Q	κ_0 (s)	Q
L2	AS auto R_{hyp}	0.0051	1200	0.0154	1200	0.0020	1200	−0.0024	1200	0.0035	1200	0.0192	1200
		0.0153	1948	0.0261	1948	0.0134	1948	0.0098	1948	0.0173	1948	0.0308	1948
		0.0128	1690	0.0308	2694	0.0221	3752	0.0204	4258	0.0277	3689	0.0223	1338
	BB (Stn f_c) R_{hyp}	0.0050	1200	0.0119	1200	0.0060	1200	0.0014	1200	0.0069	1200	0.0128	1200
		0.0142	1948	0.0220	1948	0.0152	1948	0.0115	1948	0.0162	1948	0.0224	1948
		0.0178	2573	0.0187	1621	0.0174	2273	−0.0024	1050	0.0165	1985	0.0085	1024
	BB (Evt f_c) R_{hyp}	0.0021	1200	0.0142	1200	0.0061	1200	0.0077	1200	0.0020	1200	0.0134	1200
		0.0115	1948	0.0242	1948	0.0154	1948	0.0178	1948	0.0114	1948	0.0229	1948
		0.0073	1523	0.0070	940	0.0174	2263	−0.0016	887	0.0029	1244	0.0037	863
	AS Manual R_{epi}	0.0045	1200	0.0187	1200	0.0098	1200	0.0108	1200	0.0136	1200	0.0227	1200
		0.0146	1948	0.0293	1948	0.0203	1948	0.0218	1948	0.0248	1948	0.0338	1948
		0.0188	2606	0.0253	1578	0.0275	3386	0.0196	1731	0.0235	1814	0.0235	1232
	AS Manual R_{hyp}	0.0043	1200	0.0185	1200	0.0096	1200	0.0107	1200	0.0134	1200	0.0224	1200
		0.0145	1948	0.0292	1948	0.0202	1948	0.0217	1948	0.0247	1948	0.0336	1948
		0.0187	2621	0.0253	1585	0.0275	3406	0.0196	1746	0.0233	1816	0.0225	1207
L1	AS Auto R_{hyp}	0.0048	1187	0.0334	3991	0.0200	3837	0.0201	5302	0.0214	2432	0.0231	1360
	BB (Stn f_c) R_{hyp}	0.0194	3294	0.0137	1471	0.0176	2445	−0.0080	989	0.0160	2098	0.0045	960
	BB (Evt f_c) R_{hyp}	0.0058	1649	0.0049	959	0.0150	2281	−0.0050	873	0.0005	1176	0.0013	837
	AS Manual R_{epi}	0.0191	2838	0.0254	1654	0.0290	4343	0.0192	2086	0.0216	1674	0.0229	1213
	AS Manual R_{hyp}	0.0190	2797	0.0255	1663	0.0281	3876	0.0196	2112	0.0213	1675	0.0205	1154
Average		0.0117	1724	0.0210	1512	0.0170	1987	0.0106	1482	0.0154	1620	0.0193	1256
68 per cent confidence		±0.0062	1293–2587	±0.0079	1149–2210	±0.0077	1386–3505	±0.0102	1057–2480	±0.0085	1262–2260	±0.0093	998–1693

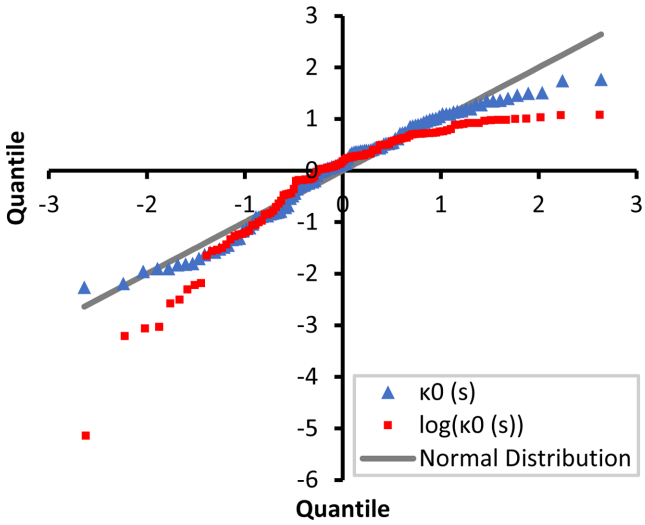

Figure 15. Quantile-quantile plot of all sites' κ_0 estimates (Table 4) using either normal (triangles) or log-normal distributions (squares).

7 DISCUSSION AND CONCLUSIONS

Seismic hazard approaches rely on knowledge of seismic attenuation at a number of stages, from magnitude determination and subsequent recurrence statistics, through to local adjustment of GMPEs for near-surface attenuation. Small changes in attenuation can have a large impact on modelled ground-motion due to its exponential nature. However, not considering the true uncertainty can lead to biases and underestimation of hazard.

The concept of κ was introduced primarily in an empirical way: a model for an observation, without full explanation of the physical basis. Numerous studies have sought to explain this phenomenon in terms of source, path, and site effects. Convincing evidence exists from borehole recordings, that the attenuation of seismic energy in the upper several hundred metres dominates the observed κ effect. However, measurements of κ rely on vast simplifications of complex wave-propagation effects. One such example is the implicit assumption of a flat Fourier spectral acceleration above the source-corner frequency: or alternatively ω^2 decay in displacement (Brune 1970). Simple models varying other source parameters (such as take-off angle) highlight that the apparent decay of displacement will not always be ω^2 (e.g. Madariaga 1976; Bethmann *et al.* 2012): the implicit assumption of the ω^2 model will therefore map epistemic variability into κ_r. Other effects such as site amplification (e.g. Michel *et al.* 2014), which may also be polarized (Burjánek *et al.* 2014) may also mask or exaggerate the measured spectral decay. Finally, we rely on the assumption of frequency-independent Q: without which attenuation parameter κ_r will vary depending on at which frequency it is measured.

A problem therefore arises from the empirical as opposed to physical definition of κ_0. The simplification of what is a complex phenomenon means that a number of sources of error enter a typical analysis. The first is measurement error: even in the case of a perfect model, we may not measure the correct value, for instance due to noise. The second is modelling error: our earthquake propagation model (from source to path to site) is a simplification and therefore what we measure may or may not be entirely related to near-surface attenuation. Examples of such issues include, but are not limited to: (1) ensuring that we properly account for the source in the analysis model in order to avoid source effects contaminating κ_0; (2) correcting for crustal attenuation or inverting directly for it along with κ_0 and (3) considering that site amplification (both local and crustal) may also mask or amplify the apparent effects of κ_0. Finally, we must consider that even in the case of a perfect model the inversion error or non-uniqueness (for example due to parameter trade-off) may introduce error in our final measurement. In reality these sources of error are inter-related, with increased noise leading to modelling and inversion problems. These errors form part of the epistemic uncertainty, that is, they could be reduced in the future given better scientific knowledge or data, but currently must be included within hazard estimation to avoid the underestimation of uncertainty and potential bias.

We showed the significant uncertainty of κ_r estimation by applying a range of methods to a common data set. Some of the differences could be explained in terms of amplification effects, and the bandwidth over which fitting occurred: targeting bandwidths in the region of amplification peaks led to over- or underestimation of κ_r. Other effects contributing to differences in κ_r between methods were related to the non-linearity of the high-frequency decay of the FAS. In fact, only one of our six hard-rock sites showed completely linear decay at high frequencies (station LLS). This site also had the lowest method to method variation. This brings to question the suitability of the κ_r (and consequently κ_0) model of attenuation for all sites. Nevertheless, in the absence of alternative models, the approach adopted here shows how, on the first order, epistemic uncertainty in κ_0 can be quantified. While certainly not exhaustively covering all sources of epistemic uncertainty, using the results of this study can help to show if selected κ_0 values in a PSHA logic tree are appropriately covering the range of values that may be observed in reality.

The uncertainty in measured spectral attenuation (κ_r) leads to significant uncertainty in any models derived from it. In this sense, and when the data justifies it, it is reasonable to model the components of κ_r in the simplest way possible: a linear fit between κ_r and distance, interpreted as a homogeneous regional crustal Q and a site-specific κ_0. Despite such a simple model we showed that resulting attenuation parameters are highly uncertain, even in the case where the match of measured κ_r between methods was better (e.g. site LLS). Fixing Q led to more consistent κ_0 between the methods, but at a cost of bias in the values, depending on the choice of Q. Here the choice of Q is difficult to justify: over the wider Swiss seismic network Edwards *et al.* (2011) showed that Q was on average 1200. However, using only the stations in this study we see lower crustal attenuation ($Q \sim 1900$). This may reflect the fact that the selected sites are located on hard rock, away from any influence of regional sedimentary basins (e.g. Swiss Molasse); on the other hand, Q across the whole of Switzerland may be affected by a variety of different geologies. The correlation between Q and κ_0 means that, when using these two parameters in applications, such as GMPEs or simulations, there should be internal consistency between them. For instance, κ_0 determined using a region-specific Q of 1900 is not compatible with the stochastic simulation model of Edwards & Fäh (2013b) or the corresponding GMPE (Cauzzi *et al.* 2015) for Switzerland that assume a nation-wide Q of 1200. Therefore, though using region-specific Q may lead to κ_0 that are more accurate on a site-to-site basis, we must ensure that their use is consistent with path attenuation in other models. A fundamental limitation of studies investigating near-surface attenuation using far-field recordings (in the absence of borehole data), therefore, is decoupling the effect of Q, which may overwhelm the influence of κ_0 at great distances. One solution would, of course, be to only use recordings of events close to the seismic stations. However, in regions of low seismicity, we often only have very few such

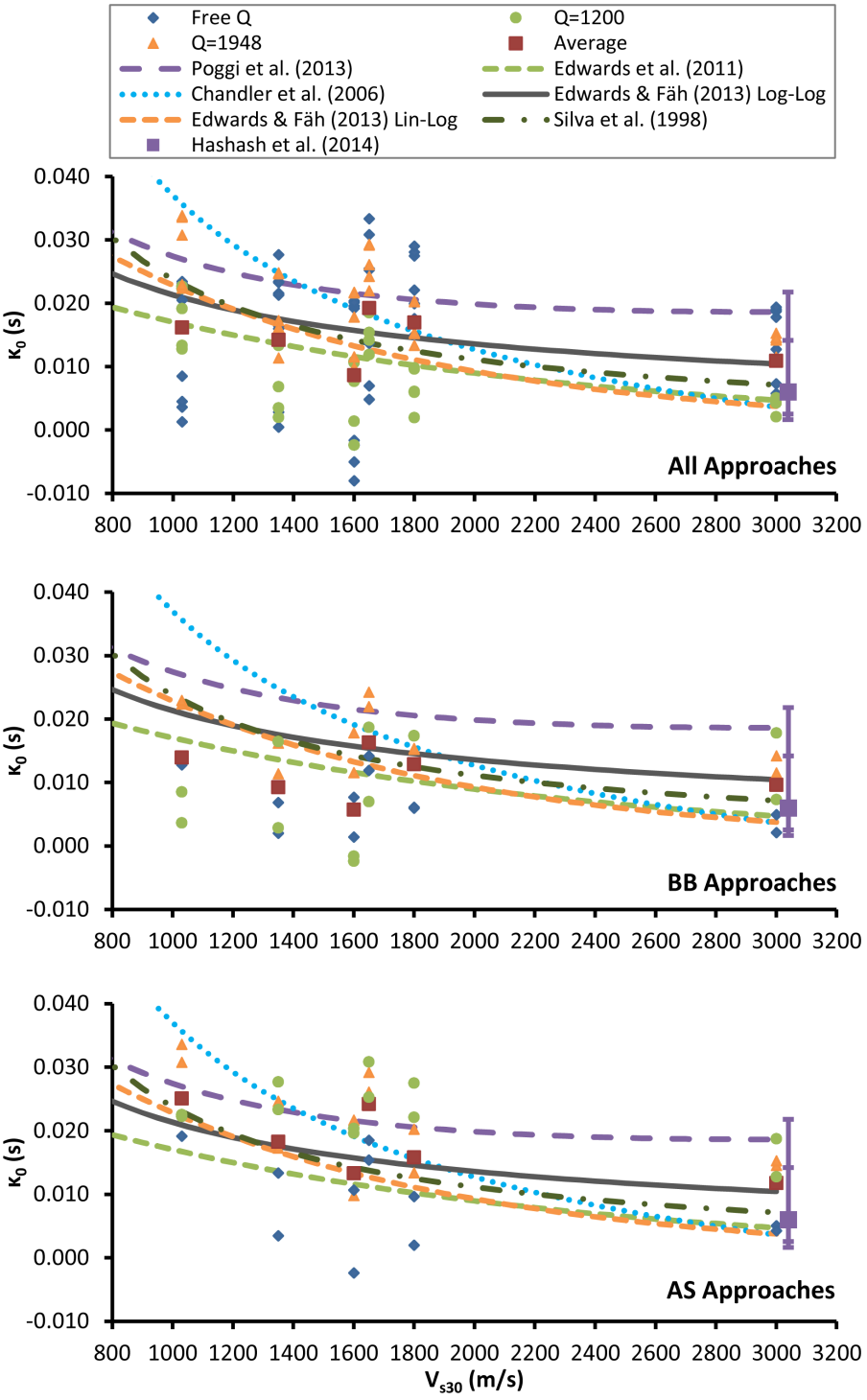

Figure 16. Comparison of existing Vs_{30}-κ_0 relations to the range of values determined in this study (Table 4). Error bars for the Hashash *et al.* (2014) reference rock model indicate 2σ and 3σ. Note that the models Silva *et al.* (1998), Chandler *et al.* (2006) and Poggi *et al.* (2013) are extrapolated beyond their maximum used Vs_{30} values of 1500, 2000 and 2100 m s^{-1}, respectively.

recordings. A significant improvement of models for determining κ_0 and κ_r, and corresponding reduction in uncertainty, will come from appropriately accounting for effects such as amplification, frequency dependence of Q and deviations from the Brune ω^2 source model. However, decoupling these effects is difficult, and the trade-offs involved may actually lead to an increased uncertainty in individual parameters such as κ_0.

Based on inter-method comparisons, the uncertainty in measured κ_r was found to be approximated by a normal distribution. The average standard deviation of κ_0 from the different approaches used in this study over all six hard rock stations was $\sigma_{epistmic}(\kappa_0) = 0.0083 \pm 0.0014$ s. Consistent with the observations that it had the most limited amplification of all sites, and that the spectral decay was completely linear beyond around 8 Hz, station LLS showed a

significantly lower epistemic uncertainty [$\sigma_{\text{epistemic}}(\kappa_0) = 0.0062$ s]. On the other hand, for the other stations significant deviations from high-frequency linear-decay, in some cases obviously produced by amplification phenomena, leads to higher uncertainty. The rather large uncertainty along with low values of κ_0 for hard rock sites means that negative values are possible. If assuming attenuation is due only to the near-surface effect of low Q materials, then negative values are physically unrealistic. However, κ_r and subsequently κ_0 are not based on physical models, rather as empirical observations of recorded data. Interpretations of these parameters in terms of physical phenomena is controversial, although the largest contribution seems to come from strongly attenuating upper soil and weathered rock layers. Observed κ_r and subsequently κ_0 may therefore be influenced by numerous other unmodelled phenomena, such as amplification, anisotropy, and variation in the source spectrum from the ω^2 model. When such variations are considered, it is possible that the measured value at hard rock sites (with comparatively low attenuation) may be negative. For example, a $\omega^{n<2}$ type source model with little near surface attenuation would lead to negative κ_r. Systematic differences in these conditions (such as a non-ω^2 source model), will therefore manifest as systematic bias in κ_0. It is important to realise that the κ_0 parameter should be used as indicative of the shape of average FAS rather than exclusively the attenuation of the near-surface. The source of the κ_0 parameter should be then be carefully considered in order to correctly implement forward modelling applications, such as in PSHA.

Finally, in the case that κ_0 cannot be directly estimated from waveform data, the correlation of κ_0 to Vs_{30} adds yet another source of significant uncertainty. This uncertainty has both aleatory components: κ_0 may not be well coupled to Vs_{30}; and epistemic components: even if it is, our measurements of, or models connecting both are limited. Existing models, unsurprisingly, were shown to pass through the large range of measured values from this study. The model of Poggi *et al.* (2013) was suggested by the authors to represent an upper bound, which seems consistent with our results (considering additionally the aleatory component of their model). On reflection, considering the results here, it cannot be said with any confidence that κ_0 scales with Vs_{30} for hard rock (specifically $Vs_{30} > 1000\,\text{m s}^{-1}$): for hazard studies it may therefore be prudent to consider a defensible range of values, as suggested by Hashash *et al.* (2014).

ACKNOWLEDGEMENTS

We thank Peter Stafford and Gail Atkinson for their reviews of this article, which have helped to significantly improve the manuscript. We also thank Glenn Biasi for helpful discussion. The records used and the site characterization data regarding the stations were provided by the Swiss Seismological Service, ETH Zürich. The research was funded at different stages by the *swissnuclear* Pegasos Refinement Project, the Swiss Federal Nuclear Safety Inspectorate (ENSI) and the French project SIGMA (http://projet-sigma.com). Signal processing benefited from SAC2008 (http://www.iris.edu/software/sac; Goldstein *et al.* 2003) and some figures were made using Generic Mapping Tools v. 3.4 (www.soest.hawaii.edu/gmt; Wessel & Smith 1998).

REFERENCES

Abercrombie, R.E., 1997. Near-surface attenuation and site effects from comparison of surface and deep borehole recordings, *Bull. seism. Soc. Am.,* **87,** 731–744.

Al Atik, L., Kottke, A., Abrahamson, N. & Hollenback, J., 2014. Kappa (kappa) scaling of ground-motion prediction equations using an inverse random vibration theory approach, *Bull. seism. Soc. Am.,* **104,** 336–346.

Anderson, J.G., 1991. A preliminary descriptive model for the distance dependence of the spectral decay parameter in Southern California, *Bull. seism. Soc. Am.,* **81,** 2186–2193.

Anderson, J.G. & Hough, S.E., 1984. A model for the shape of the Fourier amplitude spectrum of acceleration at high-frequencies, *Bull. seism. Soc. Am.,* **74,** 1969–1993.

Atkinson, G.M. & Mereu, R.F., 1992. The shape of ground motion attenuation curves in Southeastern Canada, *Bull. seism. Soc. Am.,* **82,** 2014–2031.

Bay, F., Fah, D., Malagnini, L. & Giardini, D., 2003. Spectral shear-wave ground-motion scaling in Switzerland, *Bull. seism. Soc. Am.,* **93,** 414–429.

Bay, F., Wiemer, S., Fäh, D. & Giardini, D., 2005. Predictive ground motion scaling in Switzerland: best estimates and uncertainties, *J. Seismol.,* **9,** 223–240.

Bethmann, F., Deichmann, N. & Mai, P.M., 2012. Seismic wave attenuation from borehole and surface records in the top 2.5 km beneath the city of Basel, Switzerland, *Geophys. J. Int.,* **190,** 1257–1270.

Boore, D.M. & Joyner, W.B., 1997. Site amplifications for generic rock sites, *Bull. seism. Soc. Am.,* **87,** 327–341.

Boore, D.M., Joyner, W.B. & Wennerberg, L., 1992. Fitting the stochastic omega(-2) source model to observed response spectra in western North America—trade-offs between delta-sigma and kappa, *Bull. seism. Soc. Am.,* **82,** 1956–1963.

Brune, J.N., 1970. Tectonic stress and spectra of seismic shear waves from earthquakes, *J. geophys. Res.,* **75,** 4997–5009.

Burjánek, J., Edwards, B. & Fäh, D., 2014. Empirical evidence of local seismic effects at sites with pronounced topography: a systematic approach, *Geophys. J. Int.*

Campbell, K.W., 2003. Prediction of strong ground motion using the hybrid empirical method and its use in the development of ground-motion (attenuation) relations in eastern North America, *Bull. seism. Soc. Am.,* **93,** 1012–1033.

Campbell, K.W., 2009. Estimates of shear-wave q and kappa(0) for unconsolidated and semi-consolidated sediments in eastern North America, *Bull. seism. Soc. Am.,* **99,** 2365–2392.

Cauzzi, C., Edwards, B., Fäh, D., Clinton, J., Wiemer, S., Kästli, P., Cua, G. & Giardini, D., 2015. New predictive equations and site amplification estimates for the next-generation Swiss Shakemaps, *Geophys. J. Int.,* **200,** 421–438.

Chandler, A.M., Lam, N.T.K. & Tsang, H.H., 2006. Near-surface attenuation modelling based on rock shear-wave velocity profile, *Soil Dyn. Earthq. Eng.,* **26,** 1004–1014.

De Natale, G., Madariaga, R., Scarpa, R. & Zollo, A., 1987. Source parameter analysis from strong motion records of the Friuli, Italy, earthquake sequence (1976–1977), *Bull. seism. Soc. Am.,* **77,** 1127–1146.

Deichmann, N. *et al.*, 2010. Earthquakes in Switzerland and surrounding regions during 2009, *Swiss J. Geosci.,* **103,** 535–549.

Deichmann, N. *et al.*, 2011. Earthquakes in Switzerland and surrounding regions during 2010, *Swiss J. Geosci.,* **104,** 537–547.

Douglas, J., Gehl, P., Bonilla, L.F. & Gelis, C., 2010. A kappa model for mainland France, *Pure appl. Geophys.,* **167,** 1303–1315.

Drouet, S., Cotton, F. & Gueguen, P., 2010. Nu(s30), kappa, regional attenuation and m-w from accelerograms: application to magnitude 3–5 French earthquakes, *Geophys. J. Int.,* **182,** 880–898.

Edwards, B. & Fäh, D., 2013a. Measurements of stress parameter and site attenuation from recordings of moderate to large earthquakes in Europe and the middle east, *Geophys. J. Int.,* **194,** 1190–1202.

Edwards, B. & Fäh, D., 2013b. A stochastic ground-motion model for Switzerland, *Bull. seism. Soc. Am.,* **103,** 78–98.

Edwards, B. & Rietbrock, A., 2009. A comparative study on attenuation and source-scaling relations in the Kanto, Tokai, and Chubu regions of Japan, using data from Hi-net and kik-net, *Bull. seism. Soc. Am.,* **99,** 2435–2460.

Edwards, B., Rietbrock, A., Bommer, J.J. & Baptie, B., 2008. The acquisition of source, path, and site effects from microearthquake recordings using q tomography: application to the united kingdom, *Bull. seism. Soc. Am.,* **98,** 1915–1935.

Edwards, B., Fäh, D. & Giardini, D., 2011. Attenuation of seismic shear wave energy in Switzerland, *Geophys. J. Int.,* **185,** 967–984.

Edwards, B., Michel, C., Poggi, V. & Fäh, D., 2013. Determination of site amplification from regional seismicity: application to the Swiss national seismic networks, *Seismol. Res. Lett.,* **84,** 611–621.

Fäh, D., Kind, F. & Giardini, D., 2001. A theoretical investigation of average h/v ratios, *Geophys. J. Int.,* **145,** 535–549.

Goertz-Allmann, B.P. & Edwards, B., 2014. Constraints on crustal attenuation and three-dimensional spatial distribution of stress drop in Switzerland, *Geophys. J. Int.,* **196,** 493–509.

Goldstein, P., Dodge, D., Firpo, M. & Minner, L., 2003. Sac2000: Signal processing and analysis tools for seismologists and engineers, *The IASPEI International Handbook of Earthquake and Engineering Seismology,* **81,** 1613–1620.

Hanks, T.C., 1982. Fmax, *Bull. seism. Soc. Am.,* **72,** 1867–1879.

Hashash, Y.M. *et al.*, 2014. Reference rock site condition for central and eastern North America, *Bull. seism. Soc. Am.,* **104,** 684–701.

Hough, S.E. *et al.*, 1988. Attenuation near Anza, California, *Bull. seism. Soc. Am.,* **78,** 672–691.

Hough, S.E. & Anderson, J.G., 1988. High-frequency spectra observed at Anza, California—implications for q-structure, *Bull. seism. Soc. Am.,* **78,** 692–707.

Knopoff, L., 1964. Q, *Rev. Geophys.,* **2,** 625–660.

Konno, K. & Ohmachi, T., 1998. Ground-motion characteristics estimated from spectral ratio between horizontal and vertical components of microtremor, *Bull. seism. Soc. Am.,* **88,** 228–241.

Ktenidou, O.J., Gélis, C. & Bonilla, L.F., 2013. A study on the variability of kappa (κ) in a borehole: implications of the computation process, *Bull. seism. Soc. Am.,* **103,** 1048–1068.

Ktenidou, O.J., Cotton, F., Abrahamson, N.A. & Anderson, J.G., 2014. Taxonomy of kappa: a review of definitions and estimation approaches targeted to applications, *Seismol. Res. Lett.,* **85,** 135–146.

Laurendeau, A., Cotton, F., Ktenidou, O.J., Bonilla, L.F. & Hollender, F., 2013. Rock and stiff-soil site amplification: dependency on v-s30 and kappa (kappa(0)), *Bull. seism. Soc. Am.,* **103,** 3131–3148.

Lees, J.M. & Park, J., 1995. Multiple-taper spectral-analysis—a stand-alone c-subroutine, *Comput. Geosci.,* **21,** 199–236.

Madariaga, R., 1976. Dynamics of an expanding circular fault, *Bull. seism. Soc. Am.,* **66,** 639–666.

Masuda, T. & Suzuki, Z., 1982. Objective estimation of source parameters and local q values by simultaneous inversion method, *Phys. Earth planet. Inter.,* **30,** 197–208.

Michel, C., Edwards, B., Poggi, V., Burjánek, J., Roten, D., Cauzzi, C. & Fäh, D., 2014. Assessment of site effects in Alpine regions through systematic site characterization of seismic stations, *Bull. seism. Soc. Am.,* **104,** 2809–2826.

Papageorgiou, A.S. & Aki, K., 1983. A specific barrier model for the quantitative description of inhomogeneous faulting and the prediction of strong ground motion. 1. Description of the model, *Bull. seism. Soc. Am.,* **73,** 693–722.

Parolai, S. & Bindi, D., 2004. Influence of soil-layer properties on k evaluation, *Bull. seism. Soc. Am.,* **94,** 349–356.

Poggi, V., Edwards, B. & Fäh, D., 2011. Derivation of a reference shear-wave velocity model from empirical site amplification, *Bull. seism. Soc. Am.,* **101,** 258–274.

Poggi, V., Edwards, B. & Fäh, D., 2013. Reference s-wave velocity profile and attenuation models for ground-motion prediction equations: application to japan, *Bull. seism. Soc. Am.,* **103,** 2645–2656.

Raoof, M., Herrmann, R.B. & Malagnini, L., 1999. Attenuation and excitation of three-component ground motion in southern california, *Bull. seism. Soc. Am.,* **89,** 888–902.

Renault, P., 2014. Approach and challenges for the seismic hazard assessment of nuclear power plants: the swiss experience, *Bull. Geofis. Teor. Appl.,* **55,** 149–164.

Rietbrock, A., 2001. P wave attenuation structure in the fault area of the 1995 Kobe earthquake, *J. geophys. Res.: Solid Earth,* **106,** 4141–4154.

Scherbaum, F., 1990. Combined inversion for the three-dimensional q structure and source parameters using microearthquake spectra, *J. geophys. Res.: Solid Earth (*1978–2012*),* **95,** 12 423–12 438.

Silva, W., Darragh, R., Gregor, N., Martin, G., Abrahamson, N. & Kircher, C., 1998. Reassessment of site coefficients and near-fault factors for building code provisions, technical report program element II: 98-HQ-GR-1010 Pacific Engineering and Analysis, El Cerrito, USA.

SSHAC, 1997. Recommendations for probabilistic seismic hazard analysis: Guidance on uncertainty and use of experts (NUREG/CR-6372), US Nuclear Regulatory Commission Washington, DC.

Van Houtte, C., Drouet, S. & Cotton, F., 2011. Analysis of the origins of kappa (kappa) to compute hard rock to rock adjustment factors for GMPES, *Bull. seism. Soc. Am.,* **101,** 2926–2941.

Wessel, P. & Smith, W.H.F., 1998. New, improved version of the generic mapping tools released, *EOS, Trans. Am. geophys. Un.,* **79,** 579.